UNIVERITY OF ALBERTA

PROBING SOLUTE-SOLVENT INTERACTIONS IN ETHYL 4-(DIMETHYLAMINO)BENZOATE WITH RAMAN SPECTROSCOPY

By MUNYAO MUSILLI MITAMBO 

A thesis submitted to the Faculty of Graduate Studies and Research in partial fulfillment of the requirements for the degree of Master of Science

DEPARTMENT OF CHEMISTRY

EDMONTON, ALBERTA

FALL, 2000

Abstract

A novel 4 NMR-tube holder is described for quantitative Raman and resonance Raman spectroscopy. The relative Raman intensities of a 1:1 mixture of benzene and chloroform taken in a single holder were within 6% of those of the pure solvents taken with the 4 NMR-tube holder. The resonance Raman cross-section of chromate was determined within 6% of that obtained from a single-tube holder. Raman spectra of ethyl 4-(dimethylamino)benzoate (DMABEE) were recorded in solvents of varying polarity and hydrogen bonding strength to elucidate the molecular mechanism of solute-solvent interactions in the condensed phase. Frequency shifts were observed in the vibrational frequencies of the C=O stretching, the C-O stretching and the OCO bending modes, as a function of increasing solvent acceptor number. A molecular model of DMABEE-solvent interaction is proposed based on solute-solvent hydrogen bonding and π-π interactions. These results suggest that vibrational spectroscopy provides a mode-specific measure of solute-solvent interactions.

Acknowledgments

I first thank the almighty who has brought me this far in life and seen me through its attendant trials. In you, I put my future and that of those I care about, for this is, but just another of those feeble steps you have guided me along in the journey of life. Thanks to you too for providing me with all the caring humans who have made the journey that far a possibility.

For the enabling environment that made this research work a success, my thanks to my research supervisor Dr. Glen R. Loppnow. To the members of the research group Dr. Ester Fraga, Adam M. Webb and Lucio H. Beyere who for those years were my second family, *ansanteni sana*. We have a saying in swahili, "*Milima ndio aikutani*" which translates to "Mountains are the only ones that cannot meet" so in case you turn up in Kenya, you are welcome to feel quite at home. *Nyote mwakaribiswa kwa ukarimu mkuu.* I would like to acknowledge the contributions of Dr. Shuliang Zhang to the work on the divided cell. Financial support from the Department of Chemistry during this work was greatly appreciated.

Finally and not the least, special thanks to my wife, Assumpta Mbinya Munyao who has taken care of the family during my absence, the children Helen Nyiva, Kennedy Mitambo and Martin Kasyoki. *Kwoondu wenyu na wendo, nimuvea kwa unenga vinya na wumiisyo ivinda yonthe.* God bless you always *naimusuvia mukakinyaa ithanze nthithu yila mwikuu iulu wa nthi.*

TABLE OF CONTENTS

LIST OF SCHEMES AND TABLES

TABLES

LIST OF FIGURES

Chapter 1- Introduction

1.1 Overview

The interactions between solvents and solutes is of interest in photochemical reactions and photophysical processes. A key problem has been monitoring and separating the different types of interactions, primarily because of a lack of mode specific structural probes applied to this problem. The goal of the research described in this thesis is elucidating the interactions between ethyl 4-(dimethylamino) benzoate (DMABEE) and various solvents using Raman spectroscopy as a structural, mode-specific probe.

DMABEE is a model compound for Twisted Intramolecular Charge Transfer (TICT) states. These states arise in covalently-linked donor and acceptor moieties and give rise to a dual fluorescence. Several explanations have been offered in the literature to explain the origin of the dual fluorescence but there is no consensus. The widely held view is that an internal twisting of the donor group is coupled to an electron transfer to the acceptor group.

The goal of this work is to use Raman spectroscopy in an effort to discriminate the models put forth to explain the dual fluorescence. Raman spectroscopy was the ideal choice as it is a structural, mode-specific method. As a mode-specific method, it can identify the modes that are involved in interactions between the solute and the solvent.

1.2 The Concept of Twisted Intramolecular Charge Transfer (TICT)

Lippert, et al. (1) observed that p-N,N-dimethylaminobenzonitrile (DMABN) emitted an anomalous dual fluorescence, i.e. exhibited two bands in the fluorescence spectrum. Figure 1.1 is a fluorescence spectrum of DMABN showing the two bands. One band is

similar to that observed in other benzene derivatives, while the second band occurs at lower energies and is anomalous. They proposed a solvent-induced reversal of excited states in which the anomalous band was assigned to a more polar state stabilized by solvation, i.e. the anomalous band was being emitted by a more polar species preferentially stabilized by solvation. They proposed a nomenclature that has been adopted for this dual fluorescence as $^{I}L_a$ or A* for the anomalous emission and $^{I}L_b$ or B* for the normal short wavelength emission.

Since these early studies, many other molecules have been found to behave similarly and several explanations have been proposed. Khalil, et al. (2) had proposed an excimer model based on a repetition of Lippert's experiments. They observed a third fluorescent band which was attributed to a ground-state dimer, while the anomalous band was assigned to an excimer. However, later experiments proved that their sample had been contaminated and this was the reason for the third fluorescence band.

A similar model was proposed by Kosower, et al. (3), who advocated an excited-state proton transfer as being the source of the anomalous band. In their experiments, the ratio of the A* and B* bands were examined in both protonated and deuterated solvents. The results of their experiments showed that the locally excited (LE) emission increased in the deuterated solvents. They observed a large increase in the ratio for the deuterated solvents over that for the protonated solvents. From these results, it was concluded that the A* band was due to a protonated species formed in the excited state. This model is illustrated schematically in Figure 1.2A. However, their model fails

Figure 1.1 - A spectrum of p-N,N-dimethylaminobenzonitrile (DMABN) in tetrahydrofuran showing the dual fluorescence. B* is the normal band and A* is the anomalous band.

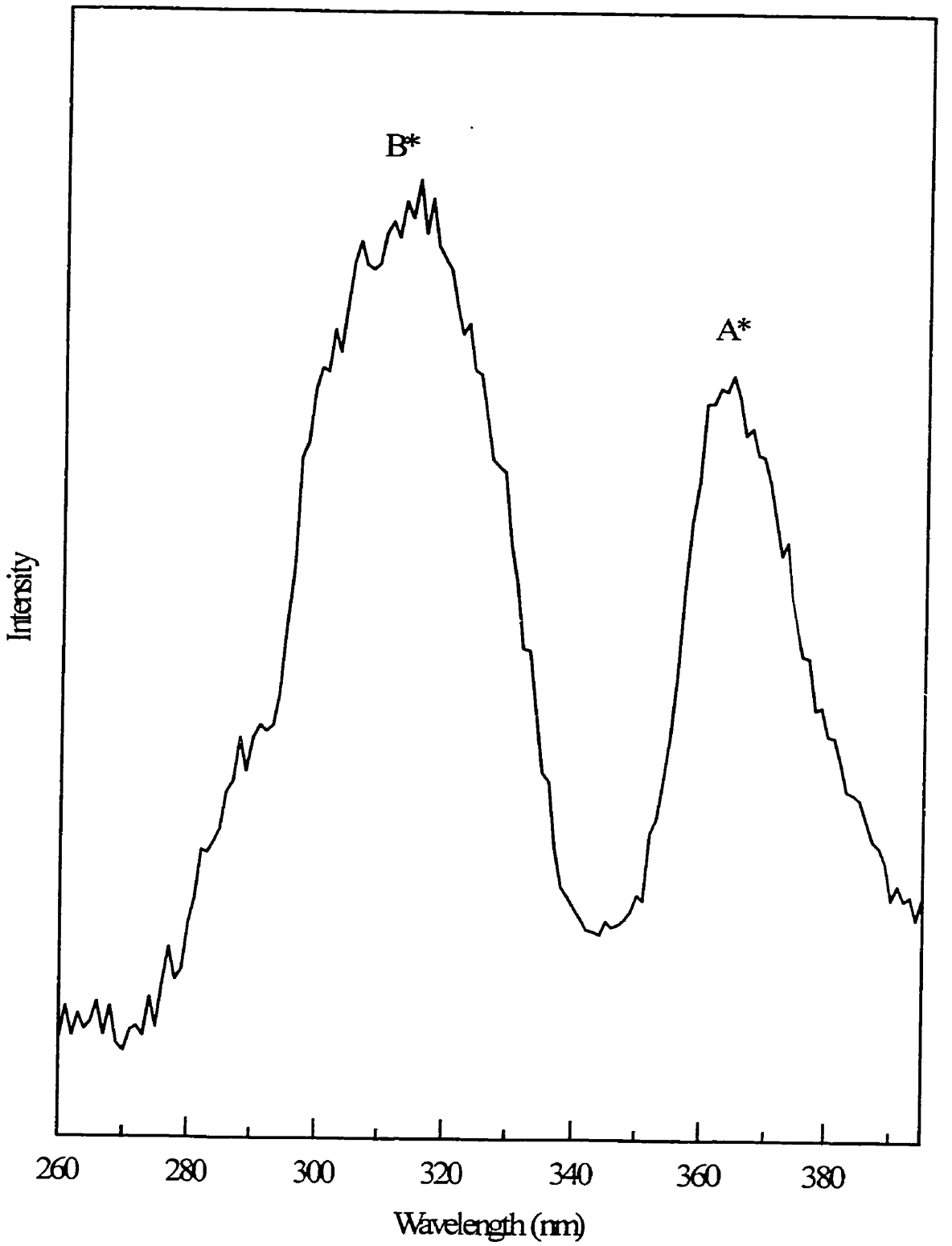
B*
A*
Intensity
260
280
300
320
340
360
380
Wavelength (nm)

Figure 1.2 - Shows a schematic illustration of models by (A) Kosower (3) and (B) Chandross (9) and Varma, et al. (10) to explain the observed dual fluorescence. See text for details.

(A)

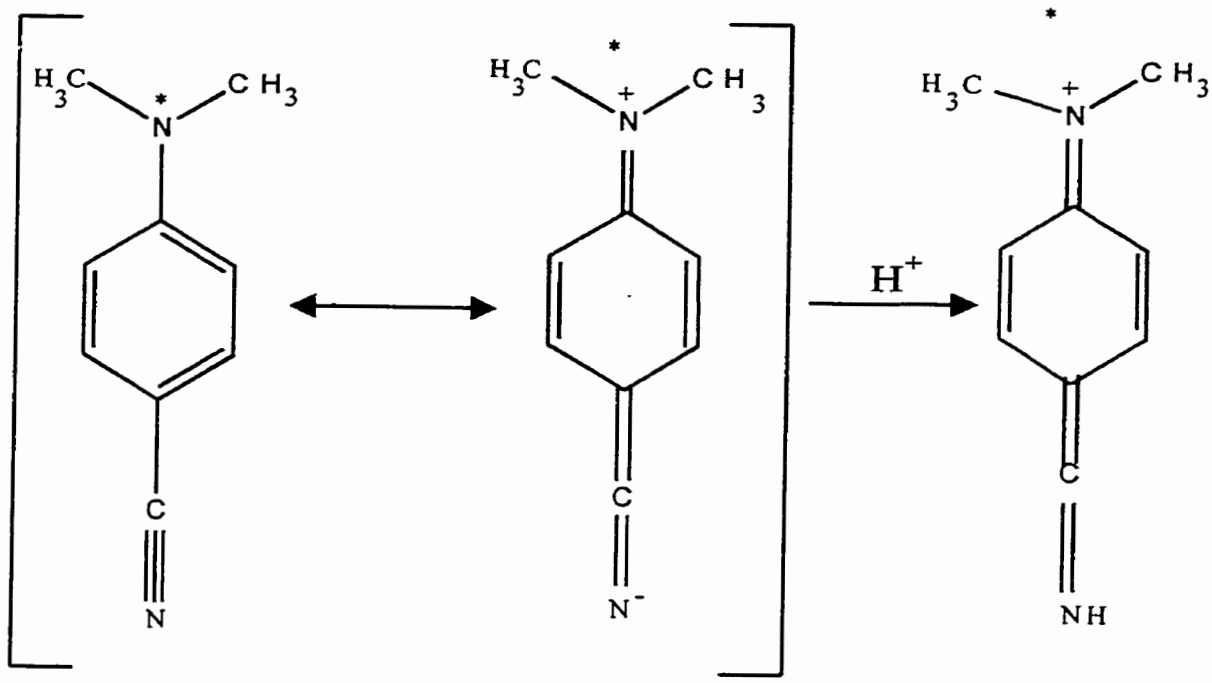

(B)

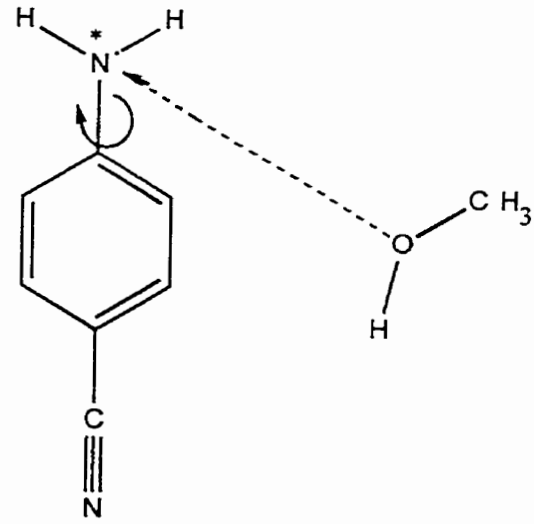

to explain the presence of the anomalous band in dried aprotic solvents (4,5), in saturated hydrocarbon solvents and in the gas phase. Though others (6,7) have observed the effect, there is no specific solute-solvent interaction necessary for the observation of dual fluorescence. In these systems, it is likely that there is a competing kinetic process which is isotope sensitive (8) and quenches the total fluorescence yield of DMABN by a factor of 10 to 100 in alcohols and water (3).

The model based on experiments of Chandross (9) and Varma, et al. (10), is similar to that of Kosower. This model explains the dual fluorescence as a photochemical reaction of excited state DMABN with solvent to form a non-covalent complex (Fig. 1.2B, ref. 10), and decays to a thermally unstable ground-state product and rapidly converts back to DMABN. However, the quenching presumably also takes place for the planar compounds **1** and **3** of Figure 1.3 (11), which exhibit no dual fluorescence and therefore, is not a feature specific to TICT states. Furthermore, when substituent groups are absent, the quenching action by protic solvents is also absent (12,13). In the early work, Chandross (9) and Varma, et al. (10) observed that the B* band of p-N,N-dimethylaminobenzonitrile was strongly quenched with increasing amounts of a polar solvent constituent in a mixture. Using a linear correlation of the intensity ratio of the two bands and the concentration of the polar solvent, they suggested that there was a 1:1 exciplex formed which was responsible for the anomalous band. This is illustrated schematically in Figure 1.2B. The binding can be attributed to a localized non-covalent interaction between the lone pair of electrons of the solvent molecule and the nonbonded electrons of the donor group in the excited state of the solute. Since it is generally observed that lone pair electrons are present on nearly all

Figure 1.3 - Model compounds synthesized by Grabowski and co-workers used to test the TICT hypothesis.

1

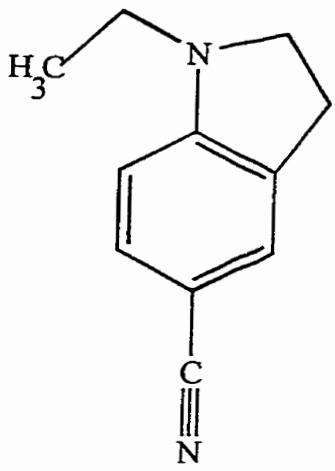

2

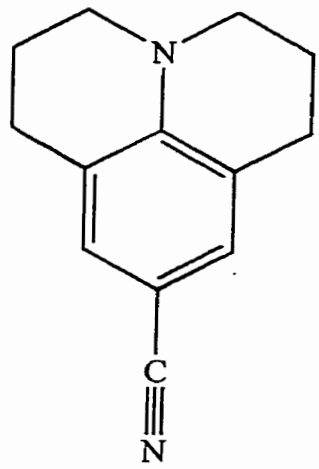

3

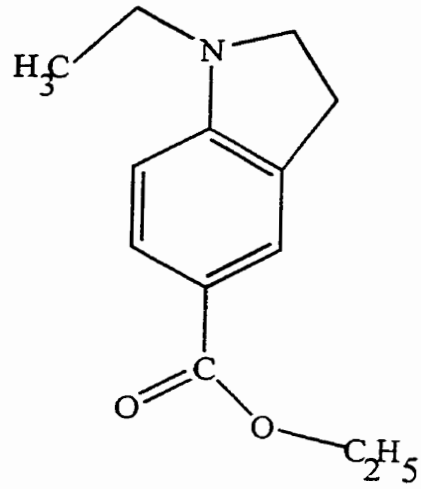

4

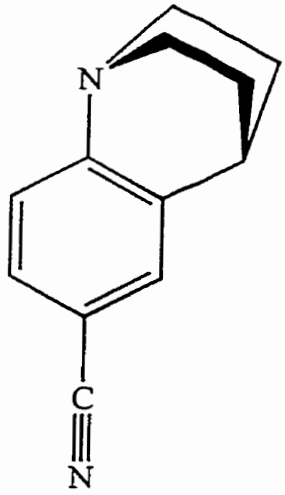

5

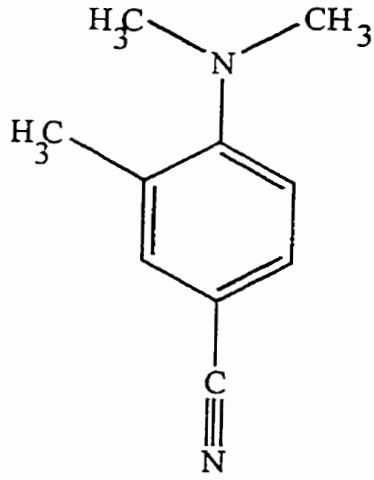

6

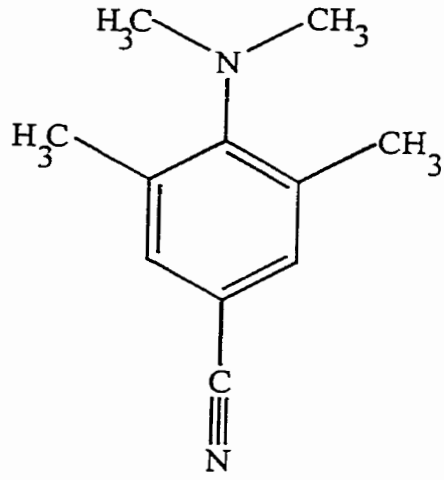

the solvents in which the TICT phenomena has been observed, this model cannot be dismissed. However, this model cannot explain TICT emission from molecules in which the donor and acceptor are already strongly twisted in the ground state and from molecules in the gas phase (4,14,15). Furthermore, though alkoxy carbonyl and cyano-substituted dialkylanilines show similar fluorescence spectra in polar solvents (16), the alkoxy carbonyls show TICT emission in aliphatic hydrocarbon solvents where such specific interactions are not possible. This model also cannot explain why the fluorescence quenching of DMABN by nitriles is of similar magnitude in high viscosity liquids as in low viscosity ones (4). This result suggests that the quenching is not linked to diffusion kinetics, as would be expected in exciplex formation, but that preferential ground-state solvation may also play a role in mixed solvents (17). Lastly, the shift to longer wavelengths of the TICT fluorescence for nearly all known molecules that exhibit TICT fluorescence, though differing largely in their structure and electronic properties, correlates reasonably well with the solvent bulk-polarity properties.

The fifth model, first proposed by Grabowski, et al. (4,18-22), is the so-called TICT model and has widely come to be associated with molecules that give dual fluorescence. In this model, the molecular systems are thought to consist of two moieties, an electron donor group, D and an electron acceptor group, A. The dual fluorescence is then explained as resulting from a locally excited state (LE) for the normal band and a charge transfer state or TICT state (CT or TICT) for the anomalous band. The structure of DMABN and an illustration of the model is shown in Figure 1.4. The novel part of this model is that the CT state can only be accessed by a torsion around some internal coordinate of the molecule. Thus, the Grabowski model states that upon excitation of

Figure 1.4 - The structure of DMABN and the model of Twisted Intramolecular Charge Transfer (TICT) states from Grabowski, et al. (4,18-22).

DMABN

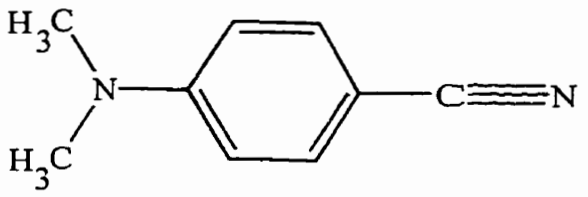

B* A*

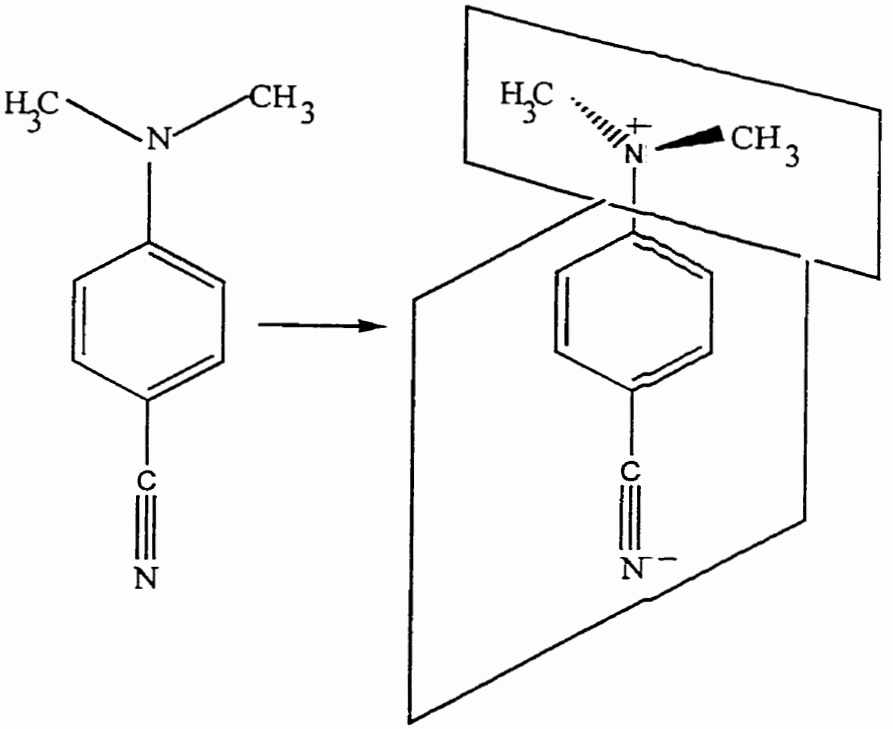

Normal Anomalous (TICT)

DMABN, B* is formed first, followed by a dynamic internal twisting of the dimethylamino group to be in a plane perpendicular to the phenyl ring and yield A*. This process is, in addition, coupled with an electron transfer from the amino group (donor, D) to the cyano group (acceptor, A).

To test their hypothesis, Grabowski and co-workers synthesized a series of molecules in which the dimethylamino group was restricted to a particular orientation with respect to the benzene plane. These molecules are shown in Figure 1.3. For bridged nitriles **1** and **2,** and ester **3,** the dialkylamino group is locked in the same plane as the benzene ring and only the B* band is reported to be observed. For molecules such as **4**, in which the dialkylamino group is perpendicular to the benzene ring, only the A* band is reported to be observed. For intermediate cases in which ortho methyl substituents were used, such as in **5** and **6**, the relative intensity of the A* band increased depending on the polarity of the solvent used. These experiments demonstrate that the occurrence of the A* band could be correlated to the dimethylamino group being able to reach an orthogonal conformation. The dependence of the band intensity on solvent polarity could be explained by the increased ability of solvent to stabilize the charged species after electron transfer. The more polar the solvent the higher the stabilization, resulting in a higher population of the A* species. Figure 1. 5 shows a schematic illustration of the potential energy surfaces for the two species in thermal equilibrium. While the TICT model is currently the favored model in discussions of dual fluorescence, it is not universally accepted. Though the experimental work by Grabowski and others overwhelmingly supports the TICT state, the mechanistic relationship between the twisting motion in the first excited singlet state and the charge-transfer reaction (TICT) has been questioned

Figure 1.5- A schematic representation of the potential energy surface of the reaction. LE is the local excited state for the nonpolar planar state. TICT is the twisted intramolecular charge transfer populated by an electron transfer process.

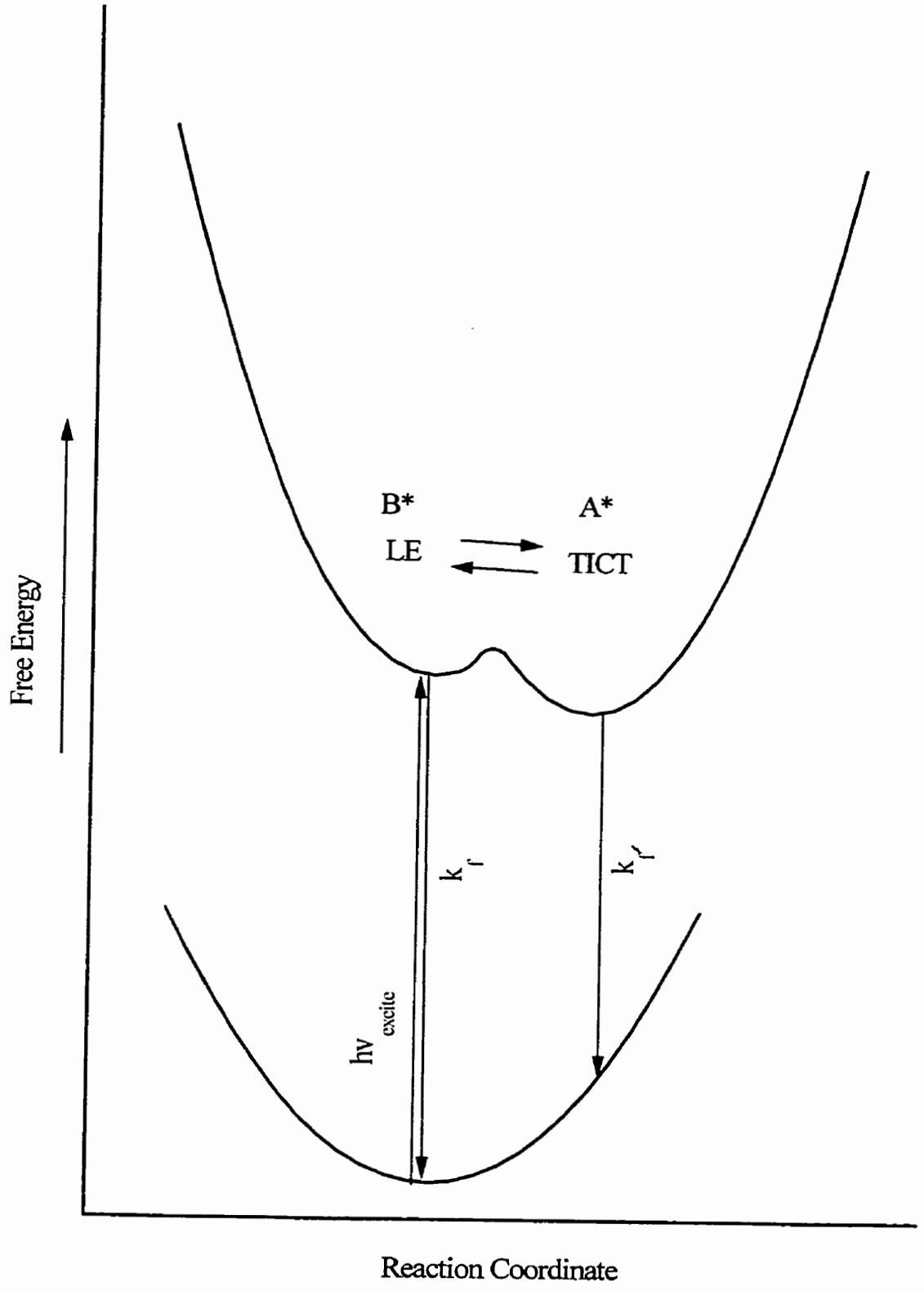
Free Energy
B*
LE
A*
TICT
k_f
$k_{f'}$
$h\nu_{excite}$
Reaction Coordinate

based on results from mass-resolved excitation spectra of jet-cooled DMABN and a number of its derivatives (23). No evidence of TICT phenomena was found in the spectra of a supersonic jet of single and monosolvated DMABN (24,25). Zachariasse, et al. (26), have shown that some of the model compounds used in support of the hypothesis are not representative. From their studies of excited-state reactions of fixed planar molecules, 1-methyl-5-cyanoindoline and 1-methyl-6-cyano-1,2,3,4-tetrahydroquinoline, they found that these underwent the same reactions as DMABN and could not support the TICT model. Furthermore, what had been assumed as a single band in the fluorescence spectrum of 3,5-dimethyl-4-(dimethylamino)benzonitrile was actually two, unresolved bands. Finally, the Grabowski model assumes that DMABN is planar in its ground state but CNDO/S3 calculations point to a non-planar ground-state configuration (18,27).

Zachariasse et al. (26) have measured the fluorescence decay for 1-methyl-5-cyanoindoline (NMCI), 1-methyl-6-cyano-1,2,4-tetradroquinoline (NMCQ), 3,5-dimethyl-4-(dimethylamino)benzonitrile (DMADBN), and 4-(dimethylamino)benzonitrile (DMABN) to study the phenomenon of dual fluorescence. In their work, they observed evidence for intramolecular charge transfer reaction via a two-state model shown in Figure 1.6A. They also found evidence that thermal exciplex dissociation took place. Though not disagreeing with the TICT model, they suggest that the dual fluorescence arises from two species, LE and an excited state rotational isomer of DMABN with an increased charge transfer character compared to the LE state.

Figure 1.6- (A) Zachariasse, et al. model for dual fluorescence. Here, k_{BA} and k_{AB} are the equilibration rate constants for the forward and backward excited-state reactions, respectively, k_f and k'_f are the radiative rate constants and τ_o and τ'_o are the fluorescence lifetimes for the LE and CT, respectively. (B) DMABEE molecular structure.

(A)

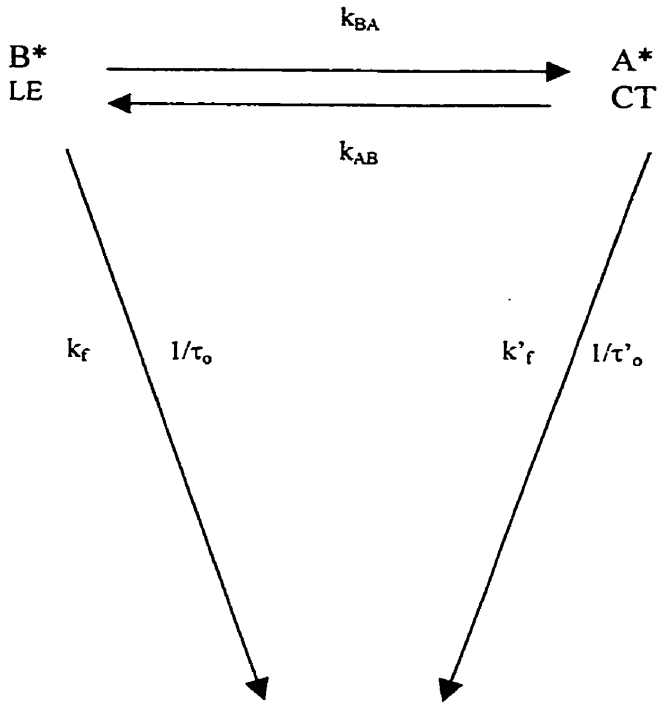

Ground State

(B)

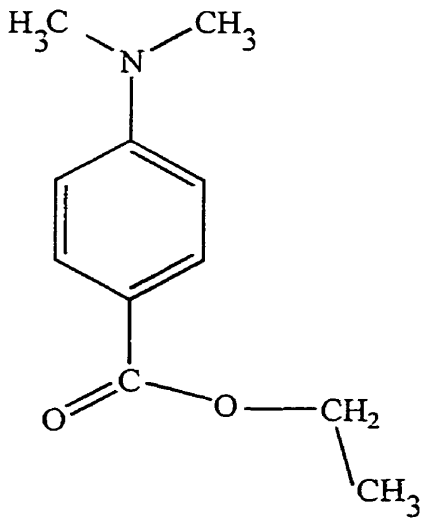

Ethyl 4-(dimethylamino)benzoate

DMABEE

In view of these various models, the goal of this work was to initiate preliminary studies with a view towards probing chemical systems and comparing the results with those produced by the different models. To achieve this, Raman spectroscopy was chosen as the spectroscopic probe. Raman spectroscopy is a vibrational technique and, as such, is sensitive to structure, dynamics, and solvent-solute interactions. TICT molecules exhibit different fluorescence behavior in different solvents. Therefore, it was the aim of this work to try to distinguish the effects of different solvents on the ground-state structure. This goal could be achieved because the vibrational frequencies provide detailed information about the geometry of the chromophore in its ground state. In this study, ethyl 4-(dimethylamino)benzoate (DMABEE) was chosen as the model for TICT states in molecules (Figure 1.6B).

1.3 Vibrational Spectroscopy

1.3.1 General

Molecules possess different types of energies such as rotational, vibrational and electronic. Each of these can be measured with the appropriate spectroscopic technique. The transition energies involved in each type are reflected in distinct regions of the electromagnetic spectrum. Energy changes involving the nuclear particles require the γ-ray region or even higher energy and those involving transition of the inner electrons of molecules require X-rays. Transitions of the valence electrons from one molecular orbital to another are probed with electronic spectroscopy, with the energies involved being in the visible and ultraviolet regions. For transitions between rotational energy levels, the

energy is in the microwave region of the spectrum and is covered under microwave spectroscopy. Energies that result in the reversal of the spin of a nucleus or an electron are covered under nuclear magnetic resonance (NMR) and electron spin resonance (ESP) spectroscopies, respectively. The vibrations of molecules will be dealt with in this work and the following sections will provide an introduction to the specific techniques used in this thesis. The energy of vibrational motions of molecules lies in the infrared region of the spectrum and can be measured using two types of spectroscopic techniques which are different but complementary, namely infrared and Raman spectroscopies.

1.3.2 Infrared and Raman Spectroscopy

Infrared (IR) and Raman spectroscopy provide similar molecular information about vibrational energies. From the two, one can obtain pure rotational, pure vibrational and rotation-vibration changes in the ground state of molecules. Although they provide similar vibrational information, they are based on quite different physical principles. Infrared spectroscopy is the absorption of energy by a molecule, ion or radical, or the emission of infrared radiation by species in excited vibrational levels. In contrast, Raman spectroscopy is based on the inelastic scattering of light energy by a molecule. In this way, the molecule can be excited to higher-lying rotational, or vibrational levels or both. The scattered photon's wavelength is detected and this forms the basis of Raman spectroscopy.

The different processes involved in the two methods leads to different gross selection rules. For a transition to be infrared active, a change in the electric dipole moment has to

occur during that vibration, whereas a change in polarizability with the vibration is required for Raman activity. The intensity of a particular transition depends on the magnitude of the change in these two properties with the vibration for the respective techniques. The two methods are complementary because of the different gross selection rules. In fact, modes may be exclusively IR or Raman active if the molecule has a center of inversion. In practice, many vibrations that are strong in the IR are weak in the Raman spectrum, and vice versa, regardless of whether the molecule contains a center of inversion. The complementarity of the two methods is useful when studying the structures of polyatomic molecules.

In this thesis, one goal was to determine the interactions between solvent and solutes with TICT states. Though both Raman and infrared spectroscopy provide vibrational information, Raman spectroscopy was chosen because it has the following advantages over IR spectroscopy: (i) selective enhancement of vibrations in a molecule can be obtained by tuning the excitation wavelength to an absorption band of the molecule in a technique called resonance Raman spectroscopy, (ii) it is possible to obtain excited-state dynamics from the resonance Raman intensities, and (iii) it is possible to obtain spectra of samples in aqueous solution without interference from the water vibrations because water is a weak Raman scatterer, whereas it absorbs strongly in the infrared.

Since Raman spectroscopy is the method of choice for this work, the remainder of this chapter will be devoted to discussing it. In Raman spectroscopy, a monochromatic light of frequency ν_0 is directed at the sample. Most of the light passes through unaffected while some is scattered by the sample molecules in all directions. The scattered light contains photons that have the same energy as the incident light (elastic scattering or

Rayleigh scattering) but also other photons of different energies. These other scattered photons have frequencies, (ν_0-ν_i) and (ν_0+ν_i), for each vibrational mode where ν_0 is the frequency of the incident photon and ν_i that of the vibrational mode (in wavenumbers). The lower frequency light (ν_0-ν_1) is known as the Stokes line while the higher frequency light (ν_0+ν_1) is referred to as the anti-Stokes line. The observed Raman frequencies depend on the rotational and vibrational energies of the particular species causing the scattering. If the energy difference between the incident photon and that of the scattered photon is $\Delta\nu$, then the Stokes lines will appear at positive $\Delta\nu$ and the anti-Stokes line will appear at negative $\Delta\nu$. The convention in Raman spectroscopy is to plot only the Stokes lines in units of cm^{-1}, where the conversion from frequency in $s^{-1}(\nu)$ to frequency in cm^{-1} (υ) is $\nu = c\upsilon$. The strongest line in the spectrum appears at ν_0 and is due to elastic scattering. It is called the Rayleigh line. A typical spectrum of carbon tetrachloride is shown in Figure 1.7.

1.3.3 Raman and Resonance Raman Spectroscopy

Raman spectra are obtained when the exciting wavelength is at an energy where the sample is transparent, while the resonance condition arises when the wavelength used to excite the Raman scattering falls within an electronic absorption band. During Raman spectroscopy, the vibrational frequencies provide information about the ground state of the chromophore. On resonance, however, selective enhancement of the vibrational modes coupled to the electronic transition occurs. This enhancement in the intensities of

Figure 1.7 - Raman spectrum of carbon tetrachloride excited at 514 nm illustrating the Stokes lines, the Rayleigh line and the anti-Stokes lines in Raman scattering.

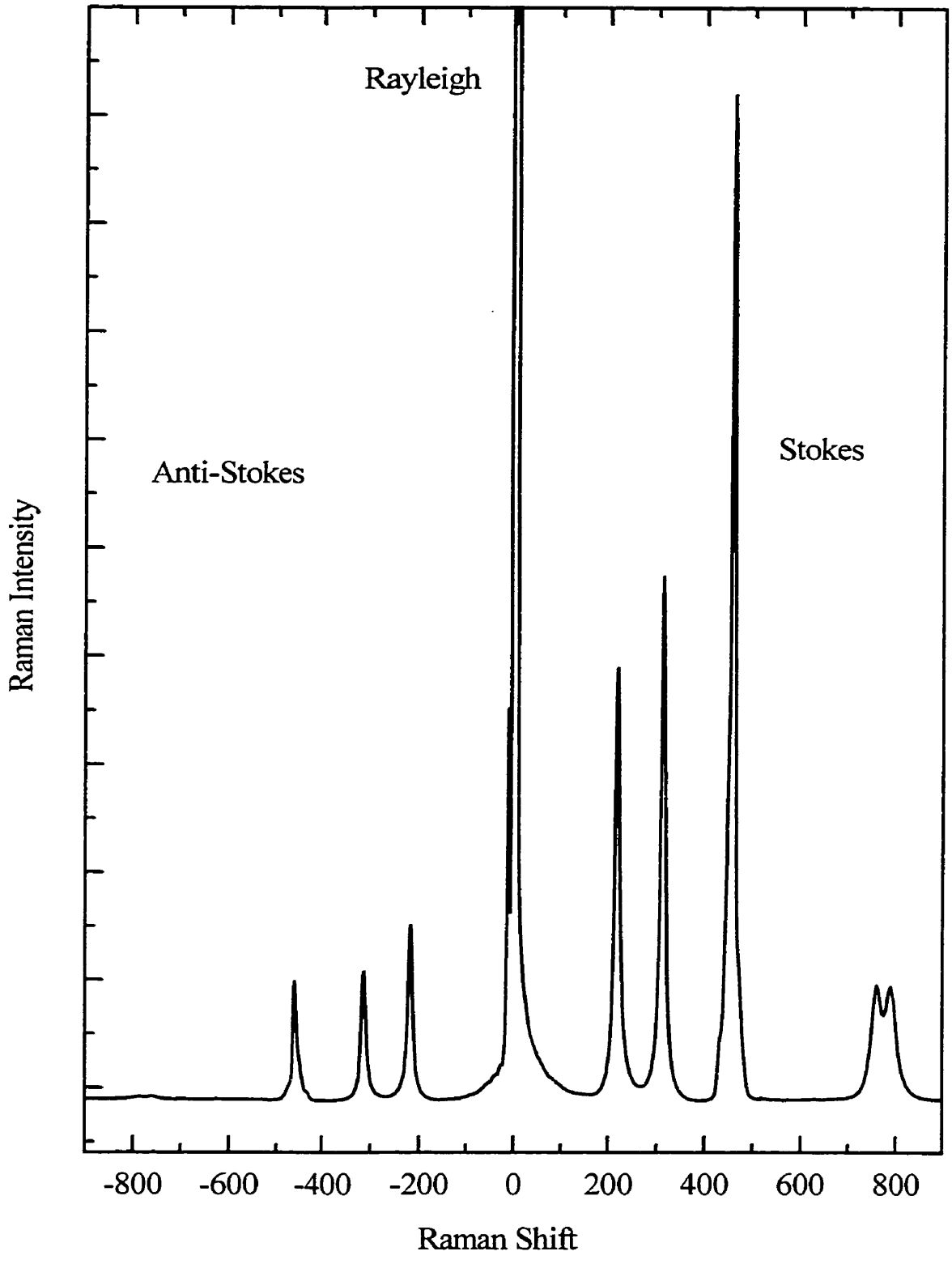
Rayleigh
Anti-Stokes
Stokes
Raman Intensity
-800
-600
-400
-200
0
200
400
600
800
Raman Shift

the vibrations that exhibit a change in equilibrium geometry upon electronic excitation can be 10^2 to 10^6 more intense than in the ordinary Raman spectrum. From the vibrational frequencies, information about the geometry and electronic structure of the absorbing species in its ground state can be obtained. In addition to this, the intensities of the Raman lines provide information about the symmetry, equilibrium geometry and the dynamics of the excited state. These two processes, showing the Stokes, Rayleigh and anti-Stokes lines for each, are illustrated in Figure 1.8. Also shown in this figure is the IR process.

1.4 Quantitative Measurement of Raman Intensities

To determine excited-state dynamics from resonance Raman intensities, it is necessary to measure the quantitative Raman cross-sections. The relationship between the observed power and the cross-section is (28):

$$P_{Raman} = I_{inc} \cdot \sigma_{Raman} \quad \text{.....(1)}$$

Where P_{Raman} is the measured Raman power, I_{inc} is the incident laser intensity and σ_{Raman} is the Raman cross-section. The Raman cross-section depends on excited-state dynamics by (28):

$$\sigma_{Raman} = \frac{8\pi e^4 E_S^3 E_L M^4}{9\hbar^4 c^4} \left| \sum_V \frac{\langle F|\mathrm{m}|V\rangle\langle V|\mathrm{m}|I\rangle}{E_V - E_I - E_L - i\Gamma} + \frac{\langle F|\mathrm{m}|V\rangle\langle V|\mathrm{m}|I\rangle}{E_V - E_F + E_L - i\Gamma} \right|^2 \quad \text{.....(2)}$$

where E_S and E_L are the scattered and incident photon energies, $|I\rangle$, $|V\rangle$, and $|F\rangle$ are the initial, intermediate, and final vibronic states, E_I, E_V and E_F are their energies, Γ is the homogeneous line width, and m_ρ is a vector component of the transition dipole length

Figure 1.8 - IR, Raman and resonance Raman spectroscopy. S_0 and S_1 represent the ground and first excited electronic states, $v_{i's}$ are the vibrational levels in each electronic state, S is the Stokes line, R is the Rayleigh line, and AS is the anti-Stokes line.

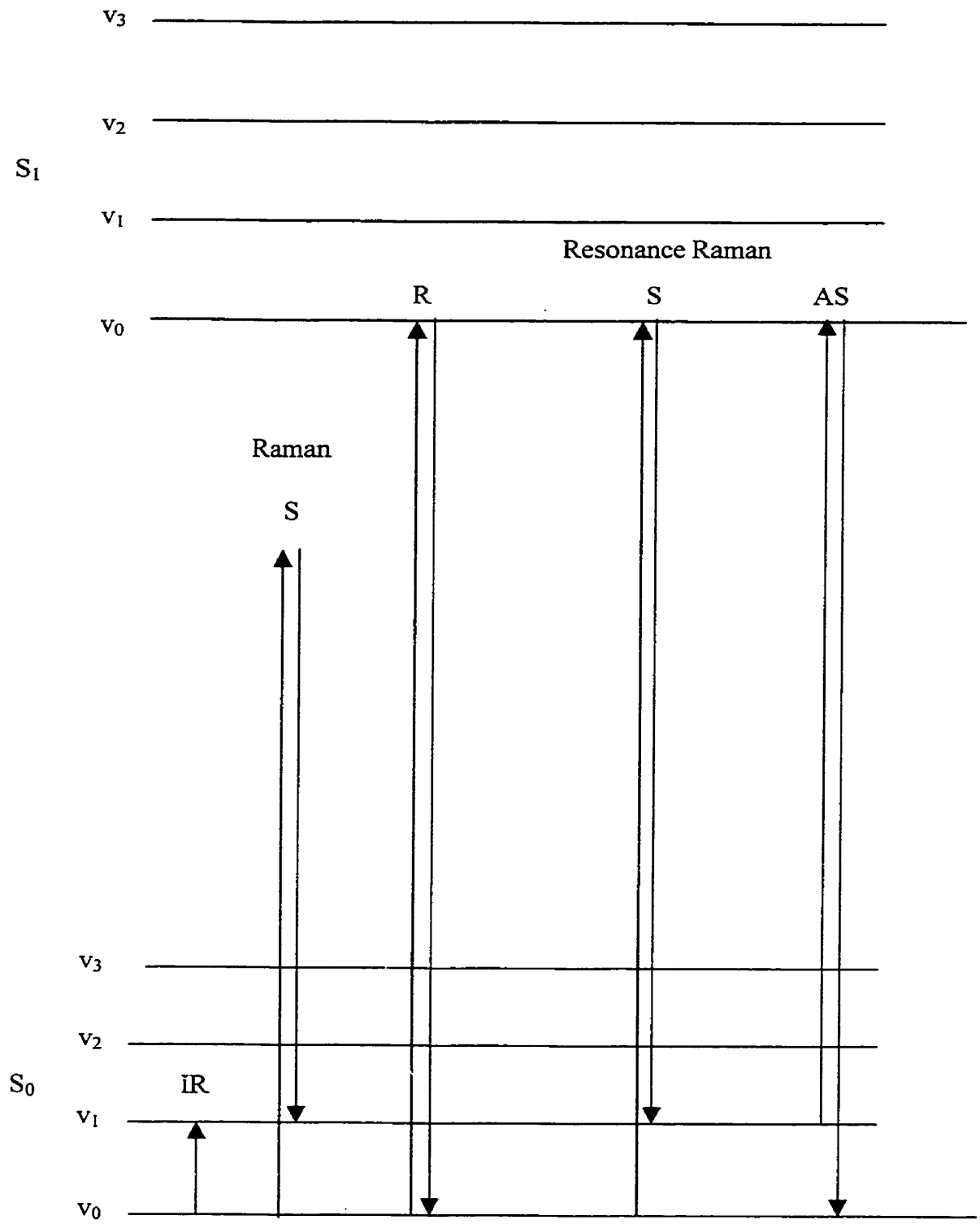
v3
v2
S1
v1
Resonance Raman
R
S
AS
v0
Raman
S
v3
v2
S0
IR
v1
v0

operator. In this equation, $\langle F|V\rangle$ and $\langle V|I\rangle$ depend only on Δ, the difference in equilibrium geometry between the ground and excited electronic states. By evaluating this equation with the measured $\sigma_{Raman,\ i\rightarrow f}$'s for each vibrational mode, a detailed description of the excited-state potential energy surface can be obtained.

Since the early experiments of Albrecht and co-workers (29), the history of Raman intensity measurements has progressed steadily with new and improved methods of measurement being developed. Mathies and Trulson (30) developed an integrating cavity method to determine the absolute Raman cross sections of the 992, 608 and 802 cm^{-1} modes of benzene, cacodylate and cyclohexane, respectively. The values obtained were in satisfactory agreement with those obtained previously by other workers (31,32). Asher, et al. (33), successfully made use of the broadband reflectance capability of barium sulfate to measure the relative Raman cross-sections of acetonitrile, sulfate, perchlorate, nitrate and benzene. Another of the early methods for quantitative measurement of absolute Raman cross-sections was developed by Champion and coworkers (34). In this work, the Raman cross-section of benzene's 992 cm^{-1} band is measured by monitoring both the incident and scattered light using a photomultiplier tube (PMT). This measurement is then followed by determination of the ratio of the Raman scattering of the mode to the total light scattering.

For accurate Raman intensity measurements, several factors have to be considered that affect the apparent intensities. One of the major problems is photoreactivity of the sample and it should be made certain that the sample does not change significantly during spectral acquisition. This problem is generally corrected for by obtaining an absorption spectrum of the sample before and after the experiment. In case of photodecomposition,

several techniques can be used to minimize it, such as the use of lower laser intensity, rapid change of the illuminated volume by flow methods or by rotation of the sample cell, cooling the sample, etc. The second problem involves the wavelength efficiency of the collecting optics, monochromator and detector. Raman intensities are typically corrected for this differential efficiency by recording the emission spectrum of a standard lamp with a known emission distribution. A correction also has to be made for the local field effect if the sample and standard are contained in solvents with different refractive indices, n, (31,35,36); using the correction factor given below.

$$L^4 = \left[\frac{n^2 + 2}{3}\right]^4 \quad \text{.....(3)}$$

If the standard and unknown are in solutions of different refractive indices, a correction must also be made for the geometric effect by multiplying by n (37). Determining the absolute Raman cross-sections from the observed intensities can be done by referencing the unknown values to a standard. Several liquids and gases have been measured accurately using various methods (30-33,38-41) and are now used as standards. The evaluation of the Raman spectral band intensities and relative cross-section is normally made with respect to a reference band. The reference band can either be from an internal standard, which is contained in the sample, or from an external standard, which sits in a separate solution. There are advantages and disadvantages of each method and these will be discussed in more detail in Chapter 2. The total absolute Raman cross-section, σ_{Raman} with the corrections, is then given by;

$$\sigma_{Raman} = \sigma_S \frac{\left[\frac{1+2\rho}{1+\rho}\right]_U}{\left[\frac{1+2\rho}{1+\rho}\right]_S} \frac{C_S E_U L_U I_U n_U}{C_U E_S L_S I_S n_S} \quad \text{.....(4)}$$

Where the subscripts U and S refer to the unknown and the standard respectively, σ_S is the standard's absolute Raman cross-section, ρ is the depolarization ratio, C is the concentration, E is the spectrometer efficiency, L is the internal field correction, n is the refractive index, and I is the relative intensity. The depolarization ratio correction is included because only a finite solid angle of collection is generally used (37).

1.5 Summary of the Research

A schematic diagram of the experimental set up is presented in Figure 1.9. In obtaining Raman spectra, three geometries of 90°, 135°, and 180° are frequently used; in this work, 135° backscattering was used. Figure 1.10 is a schematic illustration of this geometry. Chapter 2 deals with a novel four nuclear magnetic resonance (NMR)-tube holder developed for quantitative Raman and resonance Raman spectroscopy. Raman spectra obtained for both absorbing and nonabsorbing solutions using the holder are compared with those obtained with a single holder. The results of both show that the differences are within 6%, an accuracy and precision within errors normally associated with quantitative measurement of Raman cross sections. Presented in Chapter 3 are the results of preliminary Raman spectroscopy of ethyl 4-(dimethylamino) benzoate (DMABEE) in various solvents. The results demonstrate that Raman spectroscopy

Figure 1.9 - Schematic diagram of the Raman experiment.

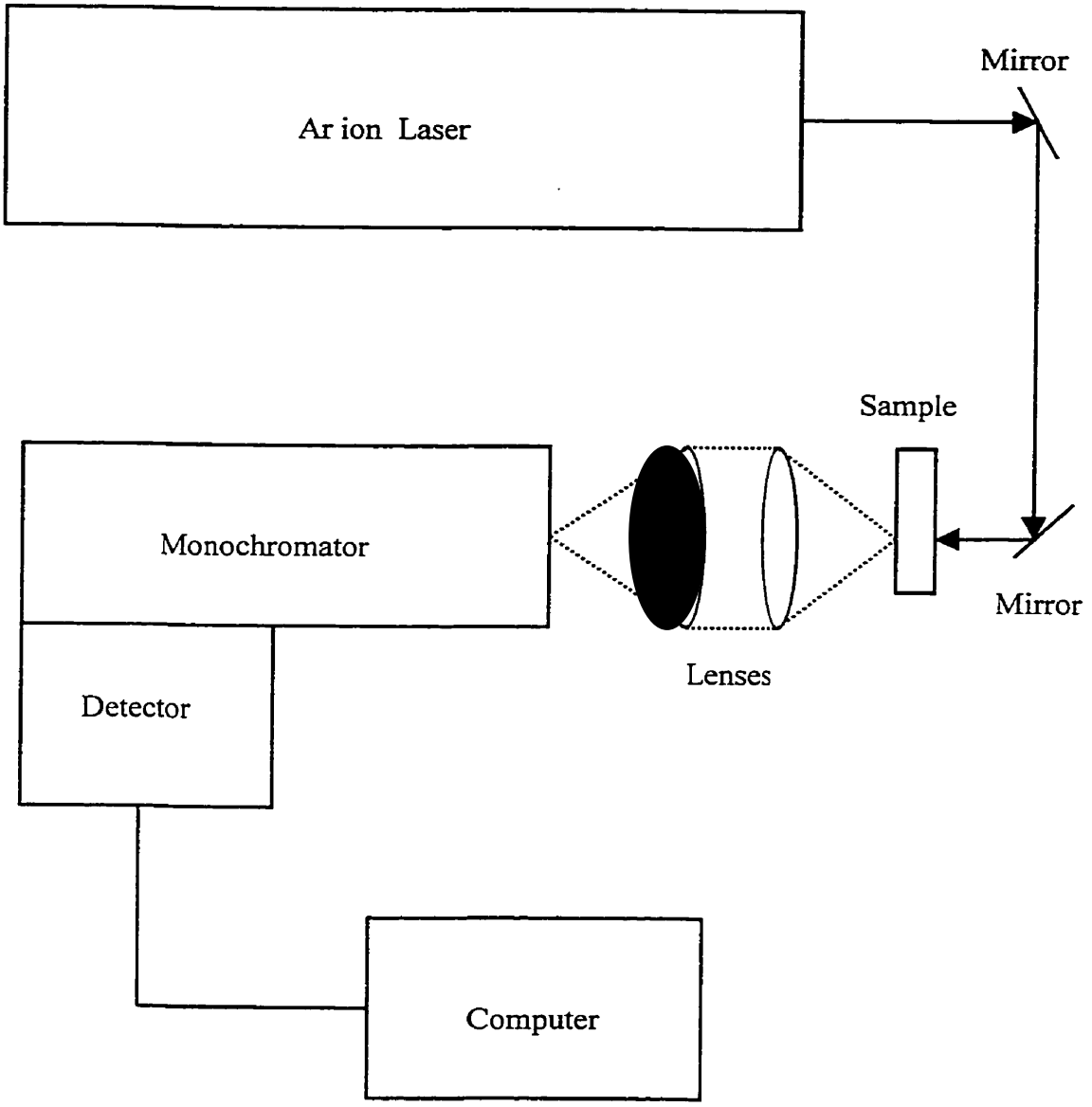
Ar ion Laser
Mirror
Sample
Monochromator
Lenses
Mirror
Detector
Computer

Figure 1.10 - 135° backscattering Raman sampling geometry used in this work.

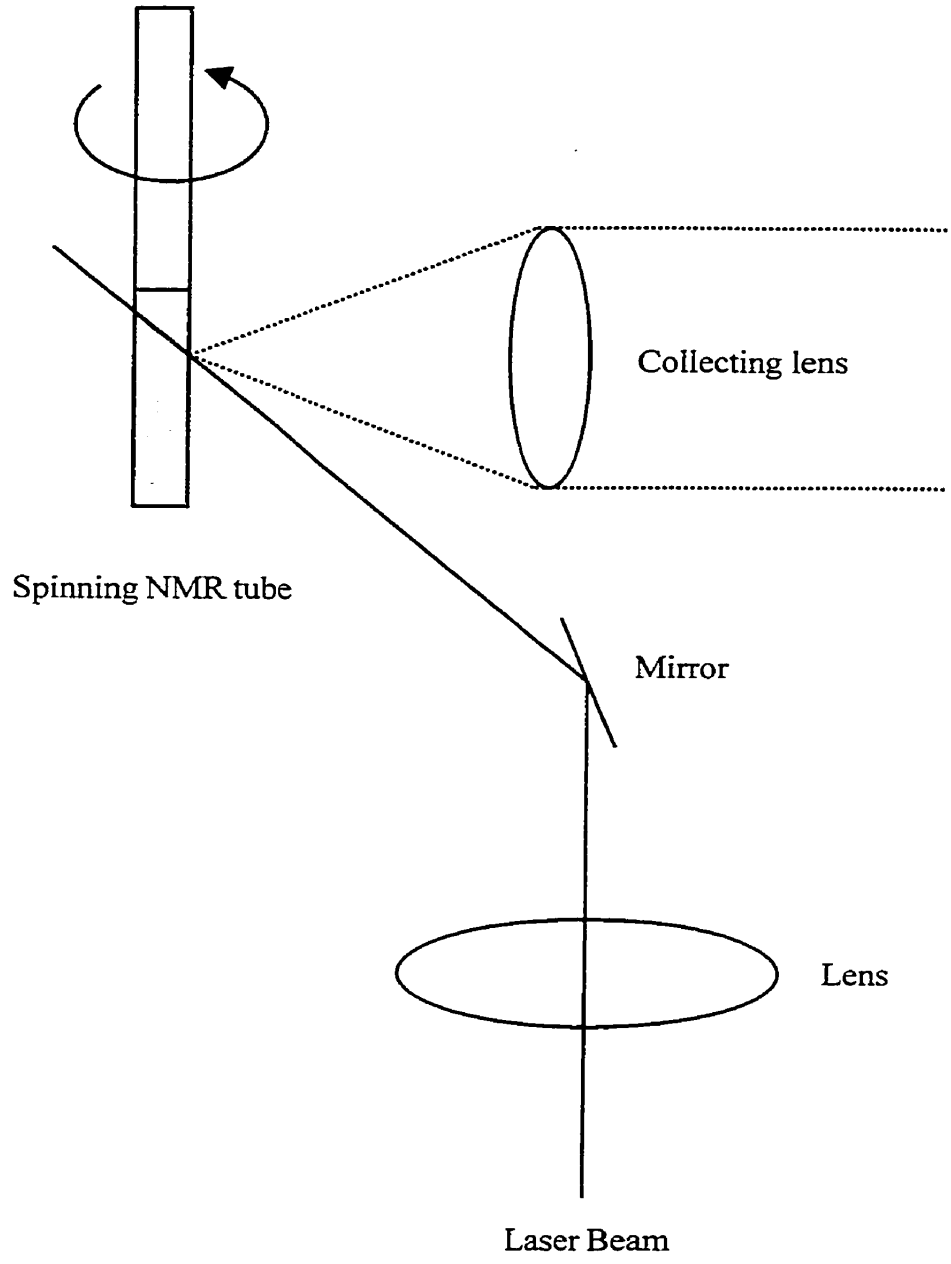
Collecting lens
Spinning NMR tube
Mirror
Lens
Laser Beam

provides a detailed molecular picture of the ground state solute-solvent interactions. Chapter 4 draws conclusions from the results presented in Chapters 2 and 3 and gives suggestions for future work.

1.6 References

1. E. Lippert, W. Lüder and H. Boos, Adv. Mol. Spectrosoc. Proc. Int. Meet. 4th 1959, 443 (1962).
2. O. Khalil, R. Hofeldt and S. McGlynn, *Chem. Phys. Lett.* **17,** 479 (1972); O. Khalil, R. Hofeldt and S. McGlynn, *J. Lumin.* **6,** 229 (1973); O. Khalil, R. Hofeldt and S. McGlynn, *Spectrosc. Lett.* **6,** 147 (1973).
3. E. Kosower and H. Dodiuk, *J. Am. Chem. Soc.* **98,** 924 (1976).
4. K. Rotkiewicz, H. Bischof, W. Baumann and N. Detzer, *Chem. Phys. Lett.* **116**, 180 (1985).
5. W. Baumann, *Ber. Bunsenges. Phys. Chem.* **80,** 231 (1976); W. Baumann and H. Deckers, *ibid.* **81**, 786 (1977); H. Deckers and W. Baumann *ibid.* **81**, 795 (1977); W. Baumann, H. Deckers, K. Loosen and F. Petzke, *ibid.* **81,** 799 (1977); W. Baumann, *J. Mol. Struct.* **47**, 237 (1978); W. Baumann, *Z. Naturforsch.* **A 36,** 868 (1981); W. Baumann and H. Bischof, *J. Mol. Struct.* **129,** 125 (1985).
6. R. Visser, C. Varma, J. Konijenberg and P. Bergwerf, *J. Chem. Soc. Faraday Trans. 2* **79,** 347 (1983).
7. K. Grellmann and K. Rotkiewicz, Lumin. Cryst. Mol. Solutions Proc. Int. Conf. 1972 (1973) Abstract 345; K. Rotkiewicz, 2nd Pol. Lumin. Conf. Vol. A (Institut of Physics, N. Copernicus University, Torun, Poland) (1974), p. 123.
8. W. Rettig, *Angew. Chem. Int. Ed. Engl.* **25**, 971 (1986).
9. E. Chandross in M. Gordon, W. R. Ware (Eds.): The Exciplex, Academic Press, New York 1975, p. 187.

10. R. Visser and C. Varma, *J. Chem. Soc. Faraday Trans. 2* **76,** 453 (1980); R. Visser, C. Varma, J. Konijenberg and P. Weisnborn, *J. Mol. Struct.* **114,** 105 (1984); R. Visser, P. Weisenborn and C. Varma, *Chem. Phys. Lett.* **113,** 330 (1985); R. Visser, C. Varma, J. Konijenberg and P. Bergwerf, *J. Chem. Soc. Faraday Trans. 2* **79,** 347 (1983); R.Visser, P. Weisenborn, C. Varma and M. de Haas, J. Warman, *Chem. Phys. Lett.* **104,** 38 (1984).

11. G. Wermuth and W. Rettig, *J. Phys. Chem.* **88,** 2729 (1984).

12. W. Rettig and M. Zander, *Ber. Bunsenges. Phys. Chem.* **87**, 1143 (1983).

13. W. Rettig and M. Zander, *Chem. Phys. Lett.* **110**, 602 (1984).

14. K. Rotkiewicz and W. Rubaszewska, *J. Lumin.* **27,** 221 (1982).

15. W. Rettig, Eur. Photochem. Assoc. Newsl. 1984, No. 21, p. 25 (conference report: Workshop on the Nature of the so called T. I. C. T. States).

16. W. Rettig and G. Wermuth, *J. Photochem.* **28,** 351 (1985).

17. E. Butty and P. Suppan, *Polym. Photochem.* **5,** 171 (1984).

18. K. Rotkiewicz, K. Grellmann and Z. Grabowski, *Chem. Phys. Lett.* **19**, 315 (1973).

19. K. Rotkiewicz, Z. Grabowski. A, Krówcynski and W. Kühnle, *J. Lumin.* **12/13,** 877 (1976).

20. K. Rotkiewicz, J. Lipinski, Z. Grabowski and H. Chojnascki, *Chem. Phys. Lett.* **70,** 449 (1980).

21. Z. Grabowski and J. Dobkowski, *Pure Appl. Chem.* **55**, 245 (1983).

22. Z. Grabowski, K. Rotkiewicz, A. Siemiarczuk, D. Cowley and W. Baumann, *Nouv. J. Chim.* **3,** 443 (1979).

23. J. Warren, E. Bernstein and J. Seeman, *J. Chem. Phys.* **88**, 871 (1988); V. Grassian, J. Warren, E. Bernstein and H. Secor, *J. Chem. Phys.* **90,** 3994 (1989).

24. T. Kobayashi, M. Futakami and O. Kajimoto, *Chem. Phys. Lett.* **130**, 63 (1986); E. Gibson, A. Jones and D. Phillips, *Chem. Phys. Lett.* **136**, 454 (1987); E. Gibson, A. Jones, A. Taylor W. Bouwman, D. Phillips and J. Sandell, *J. Phys. Chem.* **92,** 5441 (1988); J. August, T. Palmer J. Simons, C. Jouvet and W. Rettig, *Chem. Phys. Lett.* **145,** 273 (1988).

25. L. Peng, M. Dantus, A. Zewail, K. Kemnitz, J. Hicks and K. Eisenthal, *J. Phys. Chem.* **91**, 6162 (1987).

26. U. Leinhos, K. Wolfgang and K. Zachariasse, *J. Phys. Chem.* **95,** 2013 (1991).

27. J. LaFemina, C. Duke and A. Paton, *J. Chem. Phys.* **87**, 2151 (1987).

28. A. Albrecht, *J. Chem. Phys.* **34,** 1476 (1961).

29. L. Ziegler and A. Albrecht, *J. Chem. Phys.* **67,** 2753 (1977).

30. M. Trulson and R. Mathies, *J. Chem. Phys.* **84**, 2068 (1986).

31. N. Abe, M. Wakayama and M. Ito, *J. Raman Spectrosc.* **6**, 38 (1977).

32. Y. Kato and H. Takuma, *J. Chem. Phys.* **54**, 5398 (1971).

33. J. Dudik, C. Johnson and S. Asher, *J. Chem. Phys.* **82**, 1732 (1985).

34. K. Schomacker, J. Delaney and P. Champion, *J. Chem. Phys.* **85,** 4240 (1986).

35. G. Eckardt and W. Wagner, *J. Mol. Spectrosc.* **19,** 407 (1966).

36. J. Nester and E. Lippincott, *J. Raman Spectrosc.* **1,** 305 (1973).

37. J. Demas and G. Crosby, *J. Phys. Chem.* **75**, 991 (1971).

38. J. Skinner and W. Nilsen, *J. Opt. Soc. Am.* **58,** 113 (1968).

39. C. Penney, L. Goldman and M. Lapp, *Nature Phys. Sci.* **235**, 110 (1972).

40. Y. Udagawa, N. Mikami, K. Kaya and M. Ito, *J. Raman Spectrosc.* **1**, 341 (1973).

41. E. Fraga, M. Webb and G. Loppnow, *J. Phys. Chem.* **100**, 3278 (1996).

Chapter 2 - A Novel Divided Cell for Quantitative Raman and Resonance Raman Spectroscopy

Material Previously published:

M. Mitambo, S. Zhang and G. Loppnow, *Review of Scientific Instuments*, **69,** 3645 (1998).

2.1 Introduction

The determination of quantitative Raman spectral band intensities and relative cross-sections is normally made with respect to a reference band (1). The reference band can either be from an internal standard, in which a small amount of the reference substance is introduced into the sample at a known concentration, or from an external standard (1), in which the reference substance is in a separate solution. There are advantages and disadvantages of each method. The main advantage of the internal standard method, which is most commonly used (2-9), is that the chemical composition of the sample and standard is the same throughout, i.e whatever factors affect the spectrum of the species under study also affect the standard in a similar fashion. On the other hand, this method cannot be used where the standard is chemically incompatible with the species of interest or in cases where the standard may change the Raman properties under study (10-12). The use of an external standard is attractive when chemical compatibility is an issue. However, matching the spectroscopic properties of the sample and reference, and the resulting signal levels from each present formidable challenges. For example, the number of molecules in the sample and reference excited by the laser as well as the coupling of the Raman scattered light to the detector should be equivalent in the two for accurate, quantitative measurements. This constraint is particulary important in resonance Raman spectroscopy, where the incident laser beam is absorbed by the sample.

External standards have been used in Raman spectroscopy before by making use of a divided cell (13-16). The main advantage of using a divided cell is the elimination of alignment errors during sample cell substitution. Using such divided cells can be

difficult, however, in producing quantitative intensities or cross-sections. Matching the Raman signal from the two halves, having a good optical surface at the divider, and controlling the spinning axis are all potential problems.

In this chapter, a cell holder for quantitative Raman spectroscopy is described. In this novel design, a spinning holder with four nuclear magnetic resonance tubes containing the same or different solutions yields the Raman spectrum of all the components simultaneously. This design alleviates many of the problems associated with divided cells. Results are presented for Raman and resonance Raman that show this four nuclear magnetic resonance tube holder can be applied for quantitative determination of relative Raman scattering cross-section with an external standard.

2.2 Experimental

The benzene and chloroform used were of analytical grade (Fisher Scientific, Nepean, Ontario) and were used as received. Quantitative solutions of potassium chromate (Merck, Montreal, Quebec), potassium nitrate (Caledon Laboratories Ltd., Georgetown, Ontario), sodium dichromate (Fisher Scientific), and sodium nitrate (BDH Inc., Toronto, Ontario) were prepared from the analytical grade salts using distilled water.

Raman spectra of benzene and chloroform were obtained by spherically focusing 200 mW of 488 nm light from an Ar ion laser (Coherent, Santa Clara, CA) into the sample in a 135° backscattering geometry. Resonance Raman spectra of chromate and dichromate were obtained similarly by using 20 mW of 406.7 nm light from a Kr ion laser (Coherent, Santa Clara, CA). The absorption spectra were measured using a diode array

spectrophotometer (Hewlet-Packard, Sunnyvale, CA). Multichannel detection of Raman scattering was obtained with a liquid nitrogen cooled charge coupled device detector (Princeton Instruments, Trenton, NJ) connected to the first half of a double monochromator (Spex Industries, Metuchen, NJ). Spectral slit widths were 8 cm^{-1}. The spectra were analyzed by using a 486DX2-66V computer (Gateway Computers. North Sioux City, SD). The integrated band intensity was obtained by fitting the observed band with a Lorentzian or a Lorentzian-Gaussian mixture using the Spectra Calc (Galactic Industries Corp., Salem, NH) software package.

The absolute Raman cross-sections of chromate were determined from the relative integrated intensities using (6)

$$\sigma_{CrO_4^{2-}} = \sigma_{NO_3^-} \frac{\left(\frac{1+2\rho}{1+\rho}\right)_{CrO_4^{2-}} [NO_3^-]\, I_{CrO_4^{2-}} S_{i,NO_3^-}}{\left(\frac{1+2\rho}{1+\rho}\right)_{NO_3^-} [CrO_4^{2-}]\, I_{NO_3^-} S_{i,CrO_4^{2-}}} \qquad (1)$$

where σ is the cross-section, ρ is the depolarization ratio of the scattered light, $[CrO_4^{2-}]$ and $[NO_3^-]$ are the concentrations of chromate and nitrate, $I_{CrO_4^{2-}}$ and $I_{NO_3^-}$ are the integrated intensities of the chromate and nitrate vibrational bands, and S_{i,NO_3^-} and $S_{i,CrO_4^{2-}}$ are the correction factors for self-absorption of the scattered light at the nitrate and chromate vibrational frequencies, respectively. The self-absorption correction (17) was found to be $\leq 2\%$ for the experiment described here and was not considered further. The depolarization ratio for chromate was difficult to measure at 406.7 nm due to lack of a well-defined signal at the parallel orientation of the analyzer. Based on the signal-to-

noise ratio, the $\rho_{CrO_4^{2-}}$ is estimated to have an upper limit of 0.03. The nitrate cross-section was determined at the laser wavelength using (6,18)

$$\sigma_{R,NO_3^-} = \frac{8\pi}{3}\left(\frac{1+2\rho}{1+\rho}\right)K\upsilon_o\upsilon^3\left[\frac{\upsilon_e^2+\upsilon_o^2}{(\upsilon_e^2-\upsilon_o^2)^2}+C\right]^2 \qquad (2)$$

where $\rho = 0.04$, υ_o is the incident photon energy in cm^{-1}, υ is the scattered photon energy in cm^{-1}, $\upsilon_e = 51{,}940\ cm^{-1}$, $K = 9.647\times10^{-13}$ Å^2/molecule, and $C = 4.504\times10^{-10}$ cm^2. The calculated value for the 1049 cm^{-1} nitrate band cross-section at 406.7 nm is $\sigma_{R,NO_3^-} = 3.902\times10^{-12}$ Å^2/molecule.

2.3 Results and Discussion

The main objective of the work presented in this chapter was to develop a precise, accurate, and simple method for quantitating Raman and resonance Raman intensities with an external standard. After initially trying previous designs of a divided cell (13-16), problems were encountered with several aspects of the design when applied to absorbing samples. For example, the spinning axis must be coincident with the center axis of the cell to very small tolerances when highly absorbing solutions are used in a backscattering geometry, such as used here. If not, the slit image may move in and out of focus and change position, significantly decreasing the signal and altering the relative intensities of the standard and unknown Raman bands. Additionally, scattering from the divider contributes to a strong Rayleigh line, overwhelming the low frequency bands. Finally,

matching the volume and surface areas exposed to the laser from both halves within a reasonable experimental error proved difficult.

Because of these problems, a novel 4 NMR-tube holder (Fig. 2.1) was designed. The top view shows the four NMR tube cavities. The use of NMR tubes, which are designed with high tolerances, ensured equal volumes in each compartment. The 4 NMR-tube holder is made of black Delrin to reduce any stray light from the cell dividers.

During the collection of Raman scattering the holder is spun by a compressed stream of air in order to avoid sample heating. This spinning exposes the sample and the standard to the incident excitation laser beam for equal times. The window, through which the NMR tubes are exposed to the laser line, was machined to expose half the circumference of each tube. This window is necessary to avoid reflections of the incident light by the other tubes and ensures that the beam strikes a single NMR tube at a time. The NMR tube cavities have to be on a radius equidistant from the spinner axis to avoid systematic errrors that would result from changes in focal point of the Raman scattering being collected at the detector. The choice of four NMR tubes was based on the need for a design relatively insensitive to small changes in rotations around axes perpendicular to the spinning axis.

To validate the use of the new spinner, it was tested for both Raman and resonance Raman scattering methods. For the Raman experiment, a 1:1 (v/v) mixture of benzene and chloroform was used in a single NMR tube spinner and the pure solvents were used in the 4 NMR-tube spinner. The resulting Raman spectra are shown in Figure 2.2. The ratio of the integrated benzene band at 992 cm^{-1} to the integrated chloroform band at 667

Figure 2.1- The 4 NMR-tube holder design. Dimensions are given in mm.

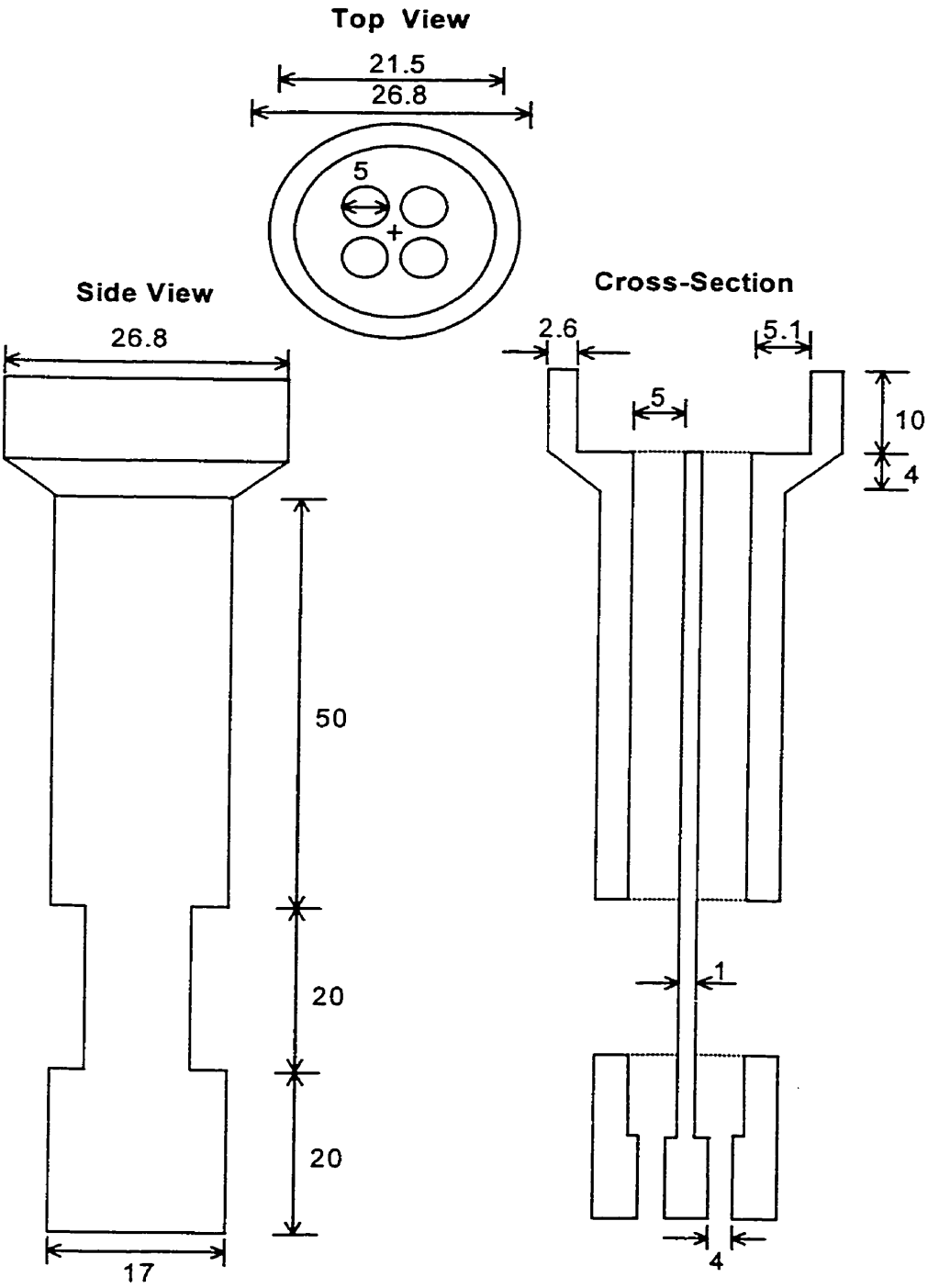
Top View
21.5
26.8
5
Side View
26.8
50
20
20
17
Cross-Section
2.6
5.1
5
10
4
1
4

Figure 2.2- A region of the Raman spectrum of benzene and chloroform excited at 488 nm. The dashed (- - - - -) line is a spectrum of the 1:1 mixture taken in a single NMR tube and the solid (——) line is a spectrum of pure benzene and chloroform in the 4-tube holder. The spectrum of the mixture has been slightly offset from that of the pure solvents.

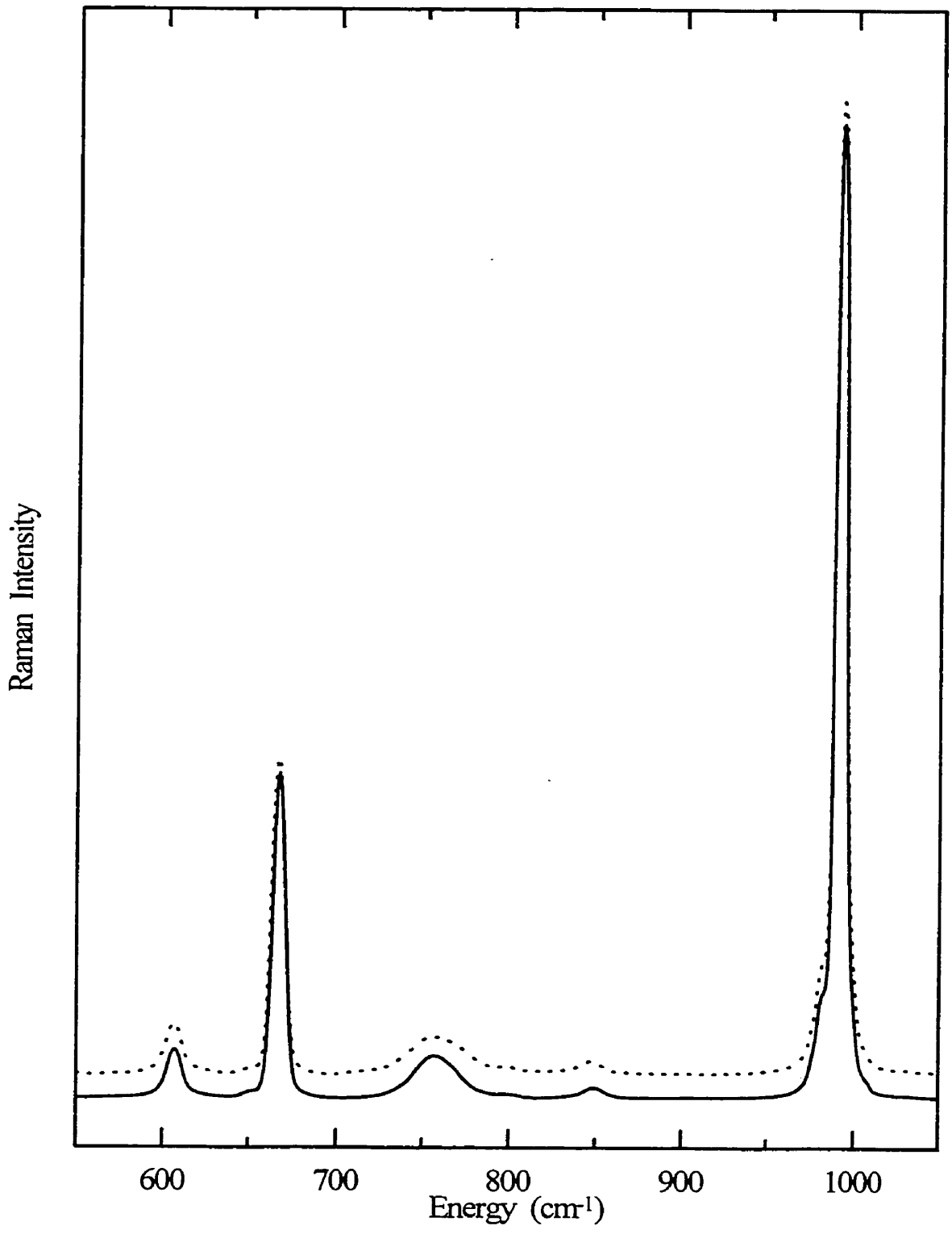
Raman Intensity
600
700
800
900
1000
Energy (cm-1)

cm^{-1} is 3.253 ± 0.004 in the single-tube spinner and 3.453 ± 0.007 in the 4 NMR tube holder. However, to compare the intensities of the pure solvents used in the four NMR tube holder and the solution used in the single tube, two corrections must be performed on the observed intensities to correct for internal field and geometric effects. For the local field factor the intensities are divided by $L^4 = [(n^2+2)/3]^4$ for each solvent (19-21). For the geometric correction, the intensities were multiplied by n, the refractive index (22). Using n = 1.5011 and n = 1.4459 for benzene and chloroform, respectively, a correction factor of 0.89 is obtained which must be multiplied by the intensity ratio to yield 3.073±0.007 for the four NMR tube holder. The experimental errors are the standard deviations in three measurements, which give a precision of 0.1% and 0.2% for the single-tube and 4-tube spinners, respectively, when used with transparent solutions. The intensities differ by 6%, which may arise from slightly lower signal-to-noise ratios in the four-tube spinner spectrum. The 6% error in accuracy is within the errors normally associated (2,4,6,8,9,14) with quantification of Raman intensities. These results demonstrated that the 4-tube spinner yields precise and accurate results for Raman spectroscopy.

For the resonance Raman experiment, the sample choice becomes much more important. To ensure that equal numbers of molecules are probed in the sample and reference, the external intensity standard must be in a solution that is absorbance matched to the sample of interest at the excitation wavelength. This is to maintain an equal optical pathlength for the incident beam through the two solutions. Criteria that an absorbance-matching species must meet are: (1) high extinction coefficients in the spectral region of interest, (2) minimum number of Raman allowed vibrations, particularly in the

vibrational region of interest, and (3) chemical compatibility with a Raman intensity standard. Typical Raman standards are cacodylate (2), dichloromethane (3), carbon tetrachloride (4), sulfate (5), nitrate (6), benzene (7,8), and cyclohexane (9). Figures 2.3 and 2.4 present the absorption and Raman spectra of suggested absorbance-matching species that meet the criteria above. The absorption spectra of these suggested absorption-matching species cover a wide spectral range, from 250 nm to 700 nm and all have high molar extinction coefficients. They have few or no Raman bands (Fig. 2.4) in the 200-1700 cm^{-1} region, are all water soluble, and do not react with nitrate and sulfate intensity standards. However, reaction was noted between cacodylate and the PtI_6^{2-} and $IrCl_6^{2-}$ absorbance matching species.

The use of this cell for absorbing samples was demonstrated on an aqueous solution of chromate. For this test, chromate was an ideal choice, since dichromate is readily available and has a similar absorption spectrum and extinction coefficient to chromate. The absorption spectra for chromate and dichromate solutions used in the experiments here are presented in Fig. 2.5A. The resonance Raman spectra of chromate with nitrate as an external (top) and internal (bottom) intensity standard are shown in Fig. 2.5B. Note that the absorbance at the laser excitation wavelength is the same in the two solutions, while it is slightly different at the chromate and nitrate scattering wavelengths. This difference in absorbance at the scattering wavelengths will necessitate a self-absorption correction for the differential absorption of the Raman scattering at the two wavelengths. Note also that the dichromate bands are relatively well separated from the chromate and nitrate bands, and should not interfere significantly with the quantitative determination of

Figure 2.3- Absorption spectra of suggested absorbance-matching solutions. The ions are: (A) $Cr_2O_7^{2-}$ ($\varepsilon_{352} = 3380\,cm^{-1}\ M^{-1}$, this work), (B) CrO_4^{2-} ($\varepsilon_{373} = 4700\,cm^{-1}\ M^{-1}$, ref. 23), (C) $IrCl_6^{2-}$ ($\varepsilon_{434} = 2560\,cm^{-1}\ M^{-1}$, ref. 24), (D) PtI_6^{2-} ($\varepsilon_{494} = 12{,}800\,cm^{-1}\ M^{-1}$, ref. 24), (E) MnO_4^- ($\varepsilon_{526} = 2440\,cm^{-1}\ M^{-1}$, ref. 23), and (F) $CoCl_4^{2-}$ ($\varepsilon_{691} = 600\ cm^{-1}\ M^{-1}$, ref. 25). The subscripts above are the absorption maxima in nm.

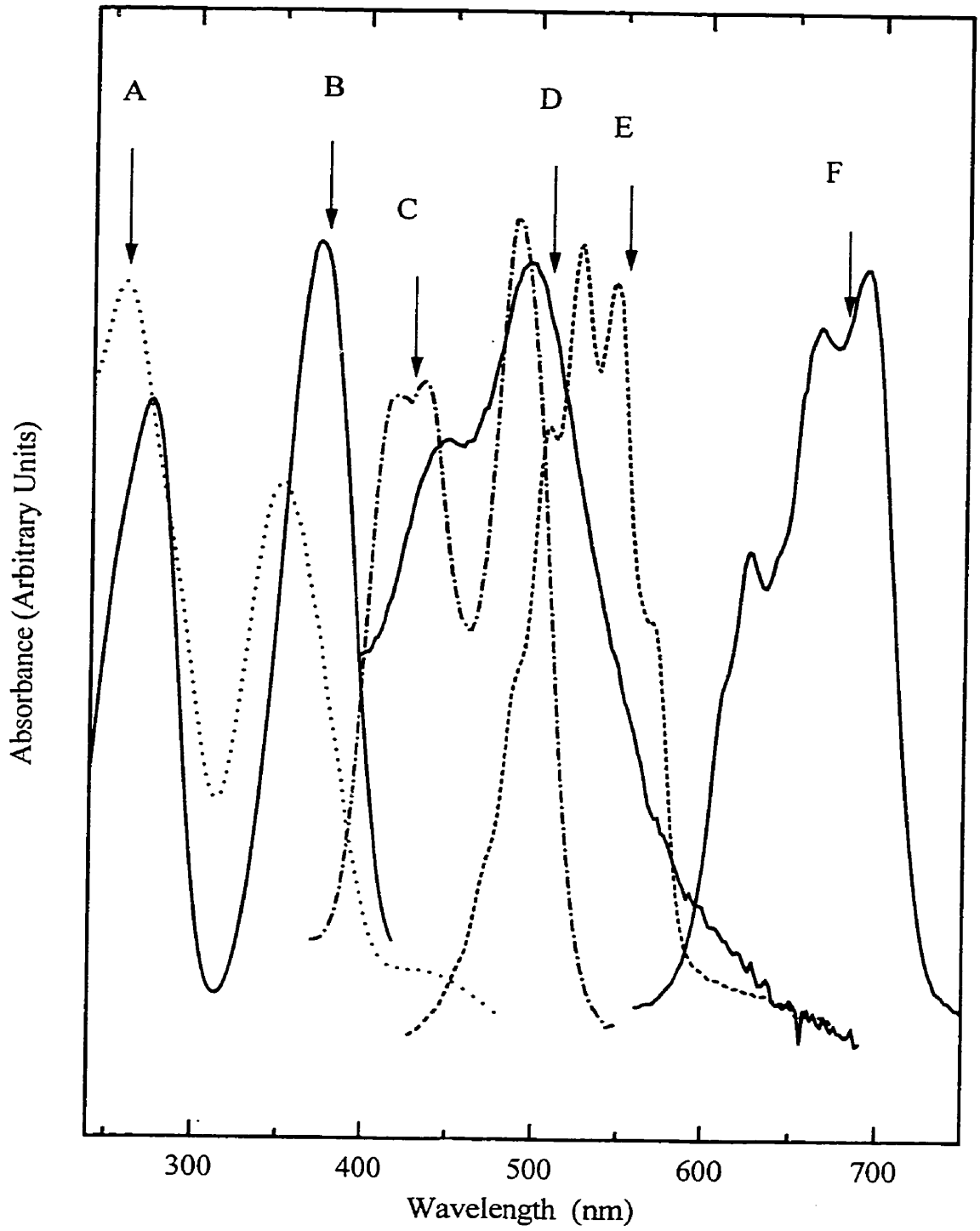
A
B
C
D
E
F
Absorbance (Arbitrary Units)
300
400
500
600
700
Wavelength (nm)

Figure 2.4- Raman spectra of (A) chromate, (B) dichromate, (C) hexachloroiridate(IV), (D) hexaiodoplatinate(IV), (E) permanganate, and (F) tetrachlorocobaltate(II) from 200 cm^{-1} to 1700 cm^{-1}. Excitation wavelength was 488 nm for chromate, dichromate and tetrachlorocobaltate(II) and 647 nm for the other spectra. The band at ~1620 cm^{-1} in (F) is due to the water solvent.

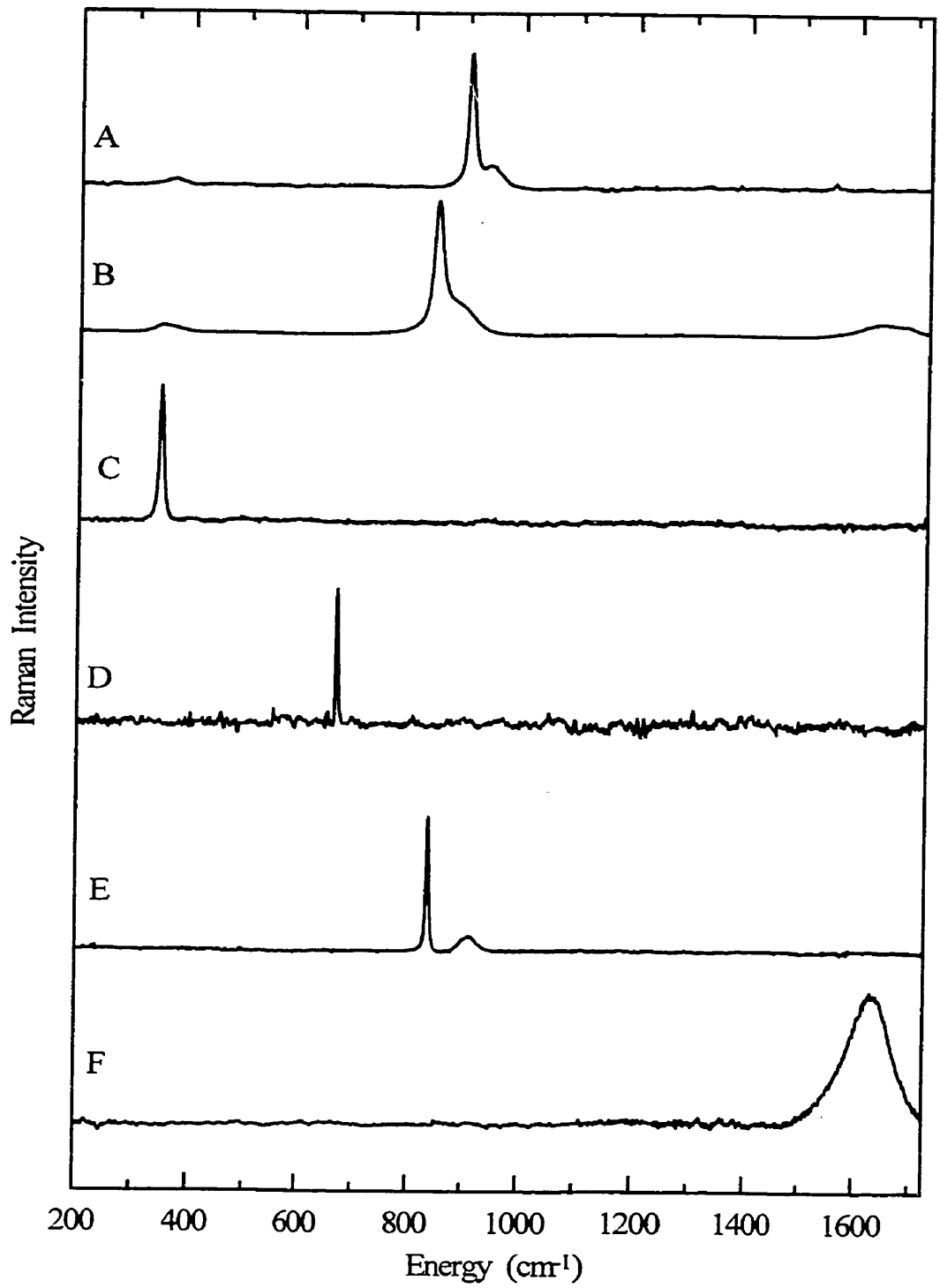
A
B
C
D
E
F
Raman Intensity
200
400
600
800
1000
1200
1400
1600
Energy (cm-1)

Figure 2.5- (A) Absorption spectra of 0.0382 M chromate and 0.0334 M dichromate solutions taken in a 0.01-cm pathlength cell. The dashed (------) line is for chromate and the solid (——) line is for dichromate. The arrows indicate the 406.7 nm excitation (laser), 424 nm chromate scattering (CrO_4^{2-}), and 428 nm nitrate (NO_3^-) scattering wavelengths used for this sample. (B) Resonance Raman spectra of chromate taken with nitrate as an external standard in dichromate solution (top) and with nitrate as an internal standard (bottom). Excitation was at 406.7 nm. The peaks are assigned to the chemical species contributing to the vibrations.

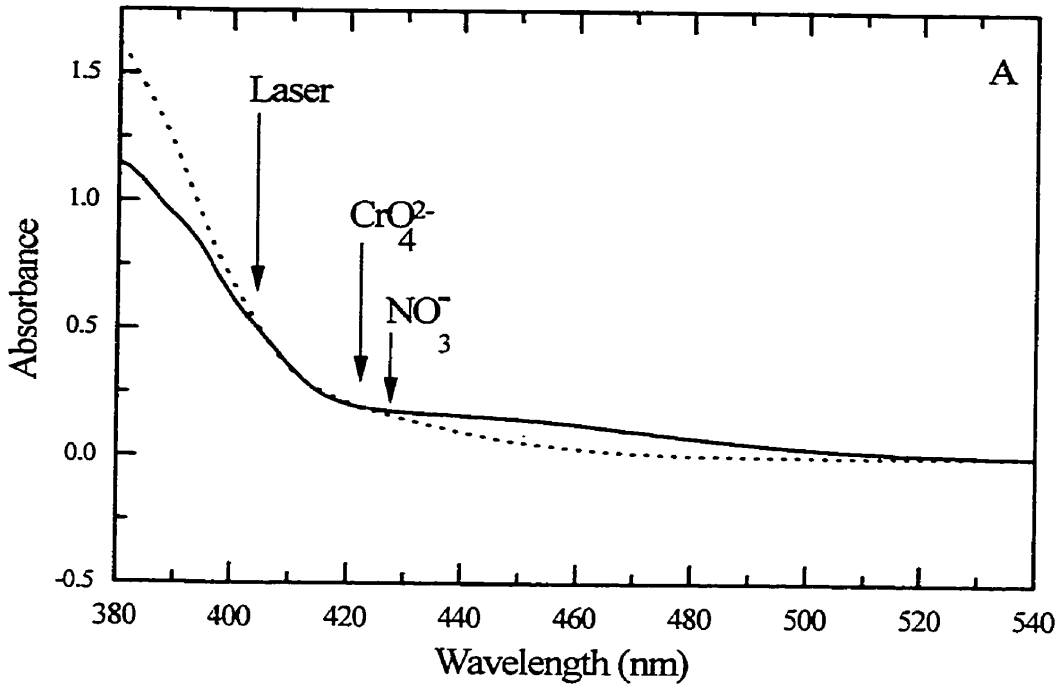
A
Laser
CrO_4^{2-}
NO_3^-
Absorbance
1.5
1.0
0.5
0.0
-0.5
380
400
420
440
460
480
500
520
540
Wavelength (nm)

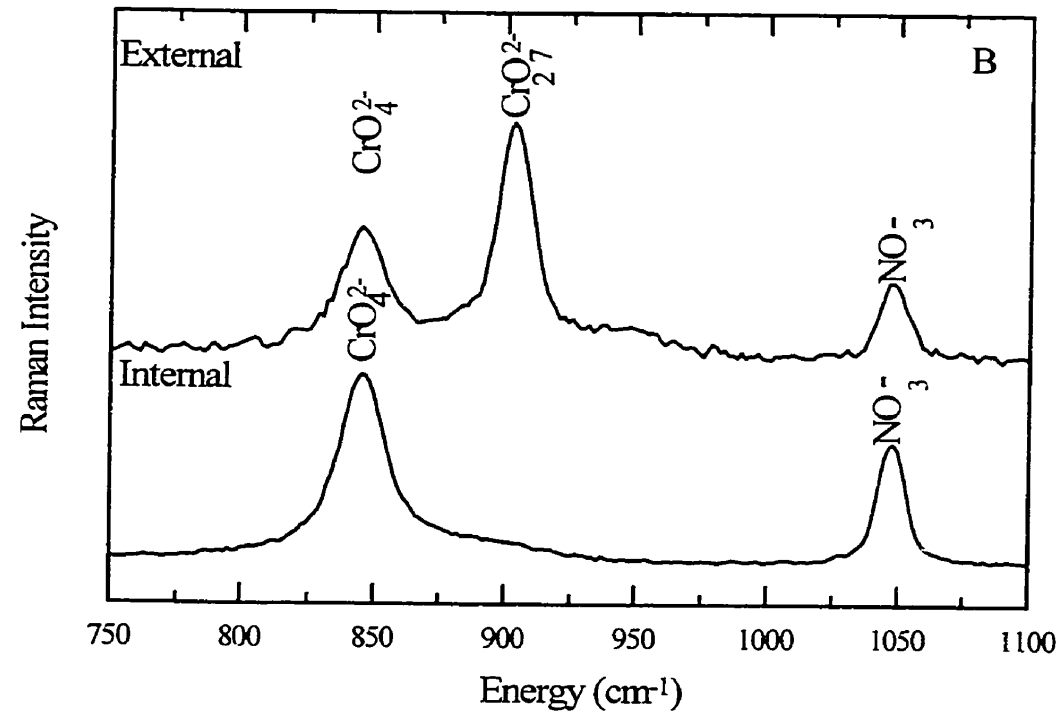
External
B
CrO_4^{2-}
$CrO_2^{2-}_7$
NO_3^-
Internal
CrO_4^{2-}
NO_3^-
Raman Intensity
750
800
850
900
950
1000
1050
1100
Energy (cm^{-1})

chromate's resonance Raman cross-section. Note also that the relative intensities of the chromate and nitrate peaks are similar in the two spectra. The resonance Raman scattering cross-sections for the 845 cm^{-1} band of chromate calculated from Equation 1 are $\sigma_{CrO_4^{2-}}$ = (9.144±0.120)×10^{-10} $Å^2$/molecule for the single tube holder and $\sigma_{CrO_4^{2-}}$ = (8.645±0.828)×10^{-10} $Å^2$/molecule for the four tube holder, a difference of 6%. Again, this error is within the precision and accuracy normally associated (2,4,6,8,9,14) with quantitation of Raman and resonance Raman cross-sections. These results demonstrate that the four-tube spinner yields precise and accurate results for both Raman and resonance Raman spectra.

2.4 Conclusion

The results presented in this chapter show that the 4 NMR-tube holder design can be used for precise and accurate measurements of both Raman and resonance Raman scattering cross-sections. This will be a useful method when the standard cannot be used internally due to chemical incompatibility or the nature of the measurement being performed. The difference in the externally- and internally-determined absolute cross-section of 6% is within the error normally associated with quantitative measurements of Raman and resonance Raman cross-sections.

2.5 References

1. T. Vickers and C. Mann, In "Quantitative Analysis by Raman Spectroscopy", Eds. (J. Grasseli and B. Bulkin, Chemical Analysis, Vol 114, John Wiley & Sons, NY. 1991), Chap. 5, p. 107.
2. E. Fraga, M. Webb and G. Loppnow, *J. Phys. Chem.* **100**, 3278 (1996).
3. B. Britt, H. Lueck and J. McHale, *Chem. Phys. Lett.* **190**, 528 (1992).
4. F. Markel, N. Ferris, I. Gould and A. Myers, *J. Am. Chem. Soc.* **114**, 6208 (1992).
5. Y. Wang, R. Purrello, S. Georgiou and T. Spiro, *J. Am. Chem. Soc.* **113**, 6368 (1991).
6. G. Loppnow and R. Mathies, *Biophys. J.* **54**, 35 (1988).
7. R. Sension, T. Kobayashi and H. Strauss, *J. Chem. Phys.* **87**, 6221 (1987).
8. K. Schomacker, J. Delney and P. Champion, *J. Chem. Phys.* **85**, 4240 (1986).
9. M. Trulson and R. Mathies, *J. Chem. Phys.* **84**, 2068 (1986).
10. M. Wohar, J. K. Seehra and P. Jagodzinski, *Spectrochim. Acta* **44A**, 999 (1988).
11. J. K. Seehra and P. Jagodzinski, *J. Raman Spectrosc.* **21**, 31 (1990).
12. M. Mitambo and G. Loppnow, *Chem. Phys. Lett.* ***261***, 691 (1996).
13. I. Tsukamoto, H. Nagai and K. Machida, *J. Raman Spectrosc.* **17**, 313 (1986).
14. H. Eysel and J. Bertie, *J. Raman Spectrosc.* **19**, 59 (1988).
15. B. Bussian and C. Sander, *Biochem.* **28**, 4271 (1989).
16. W. Kiefer, *Appl. Spectrosc.* **27**, 253 (1973).
17. J. Womack, C. Mann and T. Vickers, *Appl. Spectrosc.* **43**, 527 (1989).
18. A. Albrecht and M. Hutley, *J. Chem. Phys.* **55**, 4438 (1971).

19. G. Eckardt and W. Wagner, *J. Mol. Spectrosc.* **19**, 407 (1966).

20. J. Nester and E. Lippincott, *J. Raman Spectrosc.* **1**, 305 (1973).

21. N. Abe, M. Wakayama, and M. Ito, *J. Raman Spectrosc.* **6**, 38 (1977).

22. J. Demas and G. Crosby, *J. Phys. Chem.* **75**, 991 (1971).

23. M. Wolfsberg and L. Helmholz, *J. Chem. Phys.* **20**, 837 (1952).

24. K. Jørgensen, *Mol. Phys.* **2**, 309 (1959).

25. L. Katzin, *J. Am. Chem. Soc.* **76**, 3089 (1954).

Chapter 3- Raman Spectroscopy: A Structural Probe of Solute-Solvent Interactions in Ethyl 4-(dimethylamino) benzoate

Material previously published:

M. Mitambo and G. Loppnow, *Chemical Physics letters*, **261,** 691 (1996).

3.1 Introduction

The interactions between solvents and solutes is of interest in photochemical reaction mechanisms and photophysical processes throughout excited-state chemistry. These interactions can play a large role in determining ground-state and excited-state structure, dynamics, kinetics, and branching ratios. A key problem has been to monitor and separate the different types of interactions (hydrogen bonding, π-π stacking, electrostatic interactions, etc.) occurring between solute and solvent. The incomplete understanding of solute-solvent interactions has been exacerbated by the lack of structurally specific probes; typically, the effect of solvent on excited-state relaxation processes is followed by fluorescence lifetime measurements (1-7). While these experiments have elucidated the role of the solvents on the kinetics of excited-state relaxation processes, little direct information is provided on the specific solute-solvent interactions responsible for those kinetics. This chapter is devoted to probing the interactions between ethyl 4-dimethylaminobenzoate (DMABEE, Scheme 3.1) and solvents with Raman spectroscopy. The results presented here

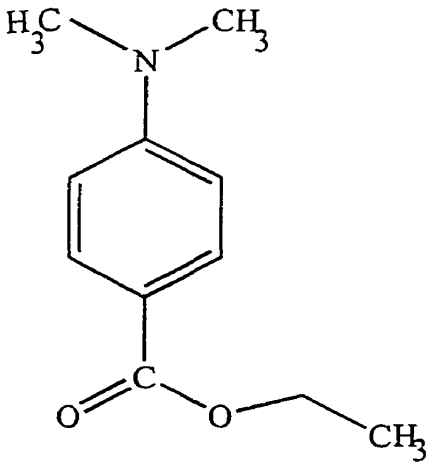

Scheme 3. 1

demonstrate that the Raman technique is a useful probe of specific solute-solvent interactions of molecules in their ground-electronic state.

In this work, DMABEE was used as the solute. This molecule exhibits solubility in a wide range of solvents and has a low-lying excited state which is purported to have twisted intramolecular charge transfer (TICT) character. TICT excited states are thought to exist in molecules which contain covalently-linked donor and acceptor moieties, and give rise to a dual fluorescence. Rotkiewicz, Grabowski, and co-workers (1-4) explained the dual fluorescence as resulting from both the locally-excited (LE) state and a TICT state, in which the molecule undergoes internal twisting of the donor group coupled with an electron transfer to the acceptor group. The final conformation of the molecule in the TICT state results, in most cases, in a 90° angle between the planes containing the donor and acceptor moieties.

The mechanisms of TICT formation proposed from fluorescence methods by various groups (4-9) all differ greatly in the role of solvent. Specifically, which property of the solvent is most important appears to be the controversial point. The classic TICT model (4) predicts an increased amount of anomalous (TICT) fluorescence in low viscosity solvents and this has been observed in time-resolved fluorescence experiments (5). An alternate view is that a solvent polarity-dependent barrier to isomerization around the donor-acceptor bond may be the primary cause of the observed solvent effect (6,7). The dual fluorescence has also been attributed to solute-solvent exciplex formation from microwave dielectric loss measurements (8,9) that show no large change in dipole moment upon formation of the putative TICT state. Calculations at the AM1, CNDO/s, INDO-CI and MNDO levels have been shown to be inadequate in elucidating the role of

solvent, as exemplified by the recent work of Samanta, et al. (10), and the references therein. It is in view of this controversy that the use of a different, structurally-specific technique to determine the role of solvent on the ground-state structure of DMABEE, namely Raman spectroscopy was deemed important.

Raman and resonance Raman spectroscopies are useful probes of solute-solvent interactions (11-13). Solvent effects manifest as frequency shifts (12), changes in vibrational linewidth (11), intensity changes, and/or increases in the allowedness of a vibrational transition due to symmetry effects on the solute by the solvent (11). Of course, solvents can also cause more profound effects, such as a change of equilibrium geometry of the ground state (13).

In this chapter, the mode-specific interaction of DMABEE with various solvents are determined by Raman spectroscopy. From assignment of these modes to specific molecular motions, it is shown that the interactions that are taking place between DMABEE and solvent occur at the carboxyl end of DMABEE. The results demonstrate that the C=O stretch frequency is a particularly useful probe of intermolecular interactions, including hydrogen-bonding and π-π interactions, and demonstrate that Raman spectroscopy provides a detailed molecular picture of the ground-state solute-solvent interactions.

3.2 Experimental

DMABEE was obtained from Aldrich (Milwaukee, WI) and used as received. Hexane, diethyl ether, benzene, 1,4-dioxane, *N,N*-dimethylformamide, acetonitrile, dichloromethane,

chloroform, *t*-butanol, 2-propanol, hexanol, pentanol, *n*-butanol, propanol, ethanol, methanol, d_4-methanol and benzyl alcohol were of analytical grade and used as received. The important solvent parameters are presented in Table 3.1.

Room-temperature Raman spectra were obtained as described previously in (14). A solvent Raman spectrum was subtracted from each solution Raman spectrum, and the resulting spectrum was frequency calibrated by measuring the Raman scattering of solvents with known frequencies (benzene, chloroform and carbon tetrachloride). The baselines were leveled by subtraction of multiple joined line segments. Reported frequencies are accurate to ± 1.5 cm^{-1}. Throughout, the frequency shift of the mode in a solvent from that in acetonitrile was used as a more precise measure of the solvent's effect on the Raman spectrum. Acetonitrile was used because its acceptor number lies in the middle of the range of solvents used. The reported frequency shifts from acetonitrile are accurate to ±0.5 cm^{-1}.

3.3 Results

The Raman spectrum of DMABEE in acetonitrile is shown in Figure 3.1. DMABEE has 81 vibrations, which are all Raman allowed in the C_S symmetry group of the molecule. Of these 81 vibrations, 22 are observed in the region of the Raman spectrum shown in Figure 3.1. Five modes show intense bands at 852, 1186, 1282, 1607, and 1698 cm^{-1}. These have all been assigned to vibrations of the benzene ring and carboxyl moiety (15). Specifically, the modes at 852, 1282, and 1698 cm^{-1} are nominally assigned as the OCO bend, C-O stretch, and C=O stretch, respectively, and the 1186 and 1607 cm^{-1} modes are assigned as

Table 3.1 Parameters of the solvents used in this study.

Solvent	AN	APAN	DN	ε	$E_T(30)$	π*
Hexane	0.0	-3.3	*	1.9	30.9	-0.081
Diethyl ether	3.9	2.5	19.2	4.3	34.6	0.273
Benzene	8.2	11.4	0.1	2.3	34.5	0.588
1,4-Dioxane	10.8	11.9	14.8	2.2	36.0	0.553
N,N-Dimethylformamide	16.0	15.1	26.6	36.1	43.8	0.875
Acetonitrile	18.9	17.3	14.1	38.0	46.0	0.713
Dichloromethane	20.4	23.2	1.0	9.1	41.1	*
Chloroform	25.1	24.9	4.0	4.8	39.1	0.760
t-Butanol	27.1	31.2	21.9	10.9	43.9	0.534
2-propanol	33.6	33.7	21.1	18.3	48.6	0.505
Hexanol	*	36.2	*	13.3	*	*
Pentanol	*	36.2	*	13.9	*	*
n-Butanol	36.8	36.2	*	17.8	50.2	0.503
Propanol	*	36.6	*	20.1	50.7	*
Ethanol	37.9	37.5	20.0	24.3	51.9	0.540
Methanol	41.5	38.8	19.0	32.6	55.5	0.586
d4-methanol	*	40.0	*	*	*	*
Benzyl alcohol	34.5	45.4	15.8	13.1	50.8	0.984

In this table AN is acceptor number (kcal mol^{-1}, ref. 16,17), APAN is the apparent acceptor number determined from the linear correlation of Fig. 3.3A, DN is donor number (kcal mol^{-1}, ref. 16), ε is the dielectric constant, (unitless, ref. 18), $E_T(30)$ is Reinchardt's number (kcal mol^{-1}, ref. 19), and π* is Kamlet and Taft's number (unitless, ref. 20). Asterisks (*) indicate undetermined values. The solvents are arranged in order of increasing apparent acceptor number.

Figure 3.1- Raman spectrum of 50 mM DMABEE in acetonitrile excited with 200 mW of 488 nm light. Asterisks (*) mark artifacts due to subtraction of the acetonitrile solvent spectrum. The intense modes at 852, 1282, and 1698 cm^{-1}, assigned to carboxyl motions, were the only solvent-sensitive modes.

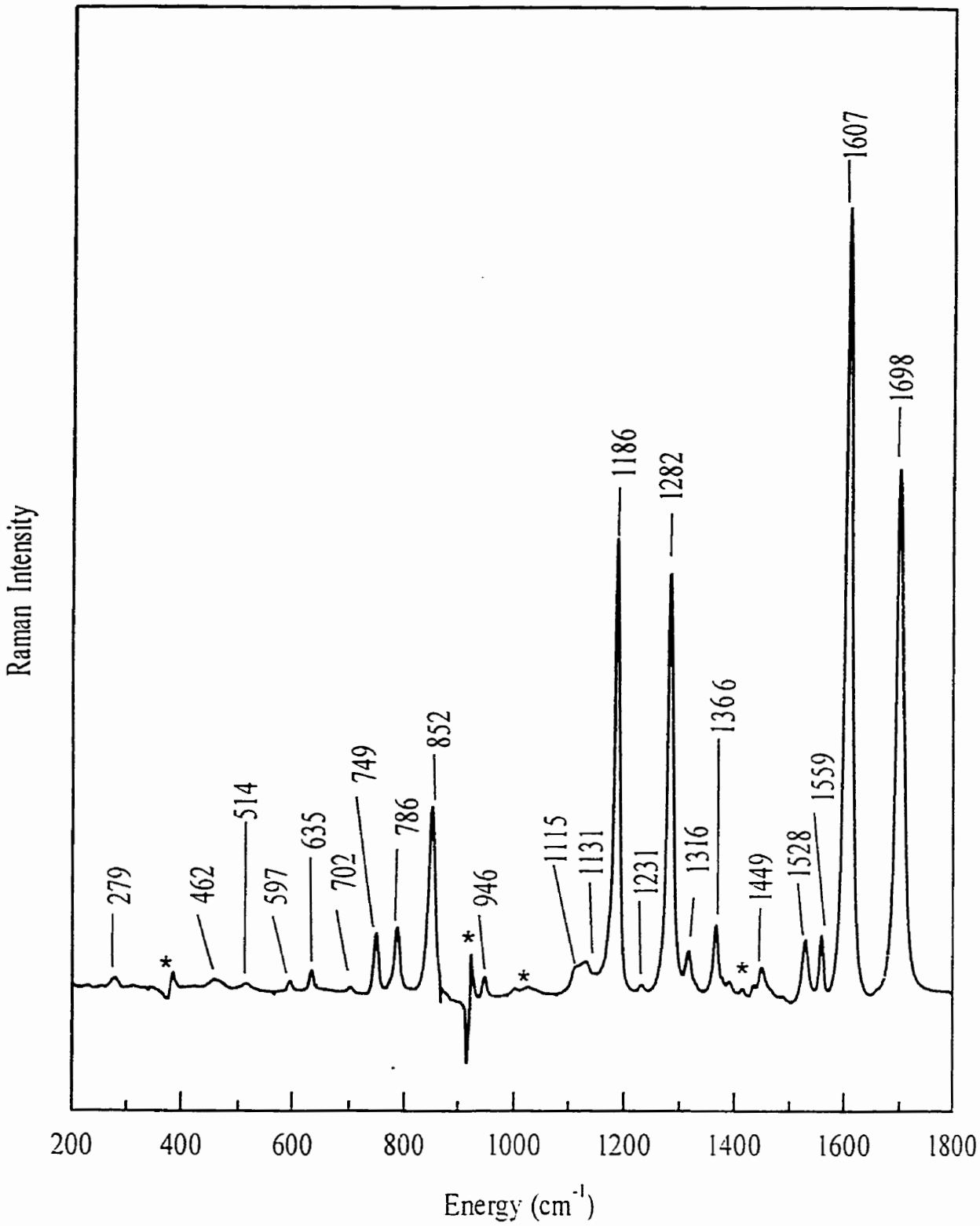
Raman Intensity
279
462
514
597
635
702
749
786
852
946
1115
1131
1186
1231
1282
1316
1366
1449
1528
1559
1607
1698
*
200
400
600
800
1000
1200
1400
1600
1800
Energy (cm-1)

the in-plane C-H bend and ring C-C stretch, respectively (14). Of all 22 modes, the three modes localized at the carboxyl end of the molecule showed sensitivity to solvent.

Figure 3.2 shows the effect of solvent on the Raman spectrum of DMABEE in the C=O stretch region. In this, and subsequent figures of this chapter, the solvents are arranged in order of increasing apparent acceptor number. Note that the C=O stretch shifts to lower frequency as the solvent acceptor number increases. This shift is accompanied by an increase in bandwidth of the C=O stretch, particularly evident in dichloromethane and chloroform. In the alcoholic solvents, the C=O stretch splits into two peaks. The splitting remains essentially constant as the acceptor number increases, except in benzyl alcohol, the solvent with the highest apparent C=O stretch frequency shift from acetonitrile. In benzyl alcohol, the splitting is reduced and the peaks have apparently started to re-coalesce into 1 peak.

To quantitate the apparent relationship between C=O stretching frequency and solvent acceptor number, a linear correlation analysis was performed (Figure 3.3A). Open circles are the data for solvents with known acceptor numbers and the triangles represent the apparent acceptor numbers as determined from the correlation line of the alcohols for which no literature values were available. Only the circles were used in the correlation analysis. The reported acceptor number for benzyl alcohol (open square) was not used in the correlation as it lies significantly off the line. The apparent acceptor numbers are reported in Table 3.1, along with literature values of the acceptor numbers and other solvent parameters for the range of solvents used in this study. The correlation between the C=O stretching frequency and solvent acceptor number (16,17) yields a correlation coefficient of 0.987.

Figure 3.2- The C=O stretch of DMABEE in representative solvents, arranged in order of increasing apparent acceptor number. Note the increase in bandwidth, with the C=O stretch shifting to lower frequencies and splitting into two peaks, as the acceptor number increases. Solvents used were: hexane (APAN = –3.3), acetonitrile (17.3), dichloromethane (23.2), chloroform (24.9), *n*-butanol (36.2), methanol (38.8), and benzyl alcohol (45.4).

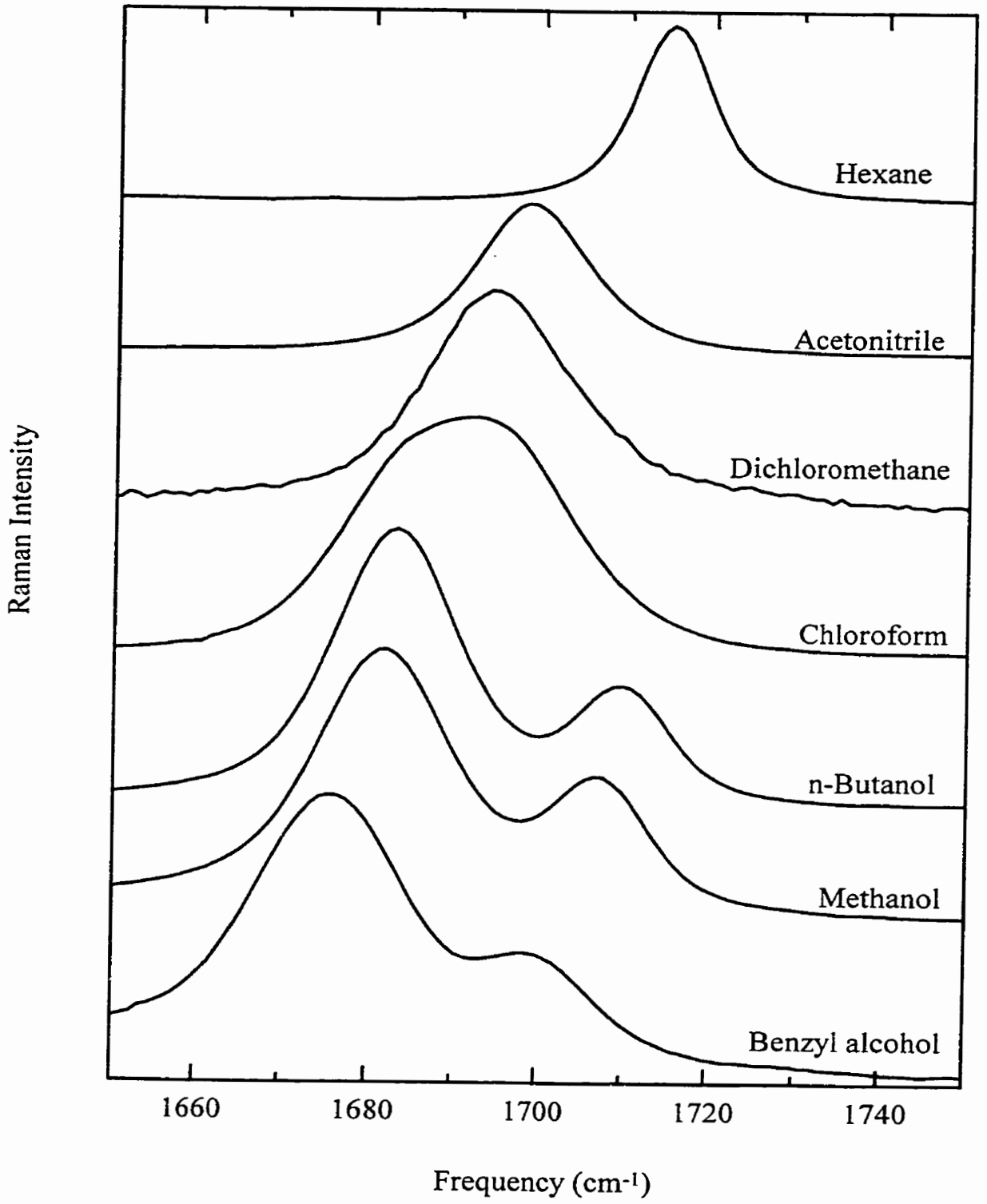
Hexane
Acetonitrile
Dichloromethane
Chloroform
n-Butanol
Methanol
Benzyl alcohol
Raman Intensity
1660
1680
1700
1720
1740
Frequency (cm-1)

Figure 3.3- Linear correlation analysis of the frequency shifts of the (A) C=O stretch, (B) C-O stretch, and (C) OCO bend of DMABEE as a function of solvent acceptor number. In all plots, open circles represent solvents with known acceptor numbers from which the correlation was done, while the triangles represent the effective acceptor number determined by the C=O stretch frequency shift correlation. The square represents the C=O stretch shift for DMABEE in benzyl alcohol using the literature solvent acceptor number. The correlation coefficients are 0.987, 0.986, and 0.969, respectively.

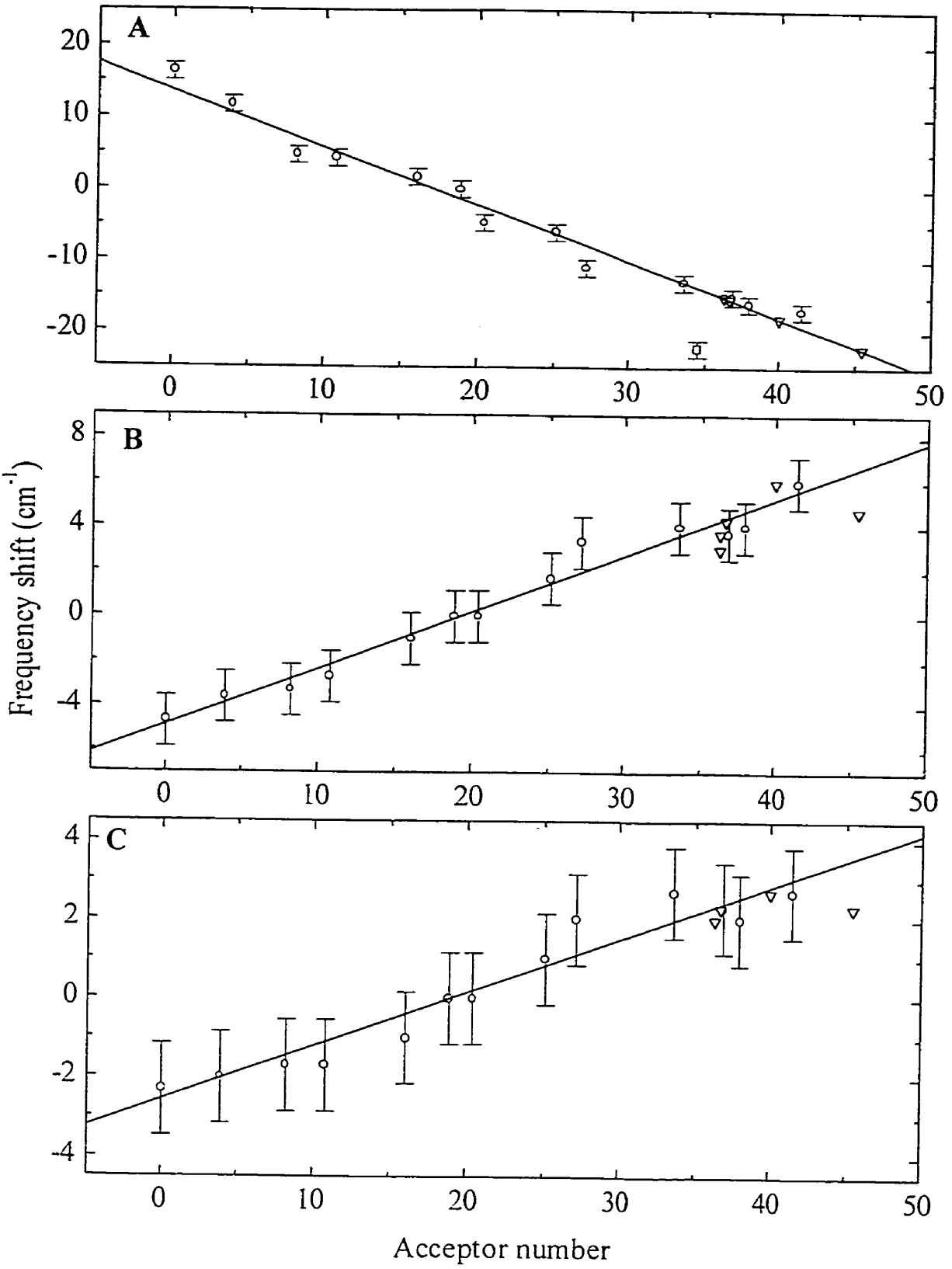
A
B
C
Frequency shift (cm^{-1})
Acceptor number

Attempts to correlate the observed frequency shifts with the other solvent parameters listed in Table 3.1 gave much lower correlation coefficients of -0.208, -0.361, -0.907, and -0.569 for the C=O stretch as a function of donor number (16), dielectric constant (18), $E_T(30)$ (19), and π^* values (20), respectively. This indicates that the acceptor number represents the solvent property that the Raman frequencies are most sensitive to.

Figures 3.4 and 3.5 show the Raman spectrum of DMABEE in the C-O stretching and OCO bending region. Contrary to the C=O stretch, the frequency of these modes increase with increasing solvent acceptor number. The C-O stretch also becomes asymmetric in the alcohols. Similar quantitative analyses of frequency shifts with solvent acceptor number yield linear correlations (Figure 3.3B and 3.3C) with correlation coefficients of 0.986 and 0.969. The frequency shifts of all three modes for DMABEE in all the solvents used in the study are collected in Table 3.2. These observed shifts in specific normal modes of DMABEE indicate that the Raman spectrum is a sensitive probe of intermolecular interactions between solute and solvent.

3.4 Discussion

The acceptor number is a measure of the solvent's ability to accept an electron pair from the solute. DMABEE was found to have three vibrations whose frequencies shifted with increasing solvent acceptor number. These were the C=O stretch around 1690 cm^{-1}, C-O stretch around 1280 cm^{-1}, and OCO bend around 850 cm^{-1}. The following model is proposed to describe the molecular nature of the observed behavior (Figure 3.6). Interaction between the solvent (hydrogen bond electron acceptor) and the DMABEE molecule

Figure 3.4- As in Figure 3.2, but for the C-O stretch of DMABEE.

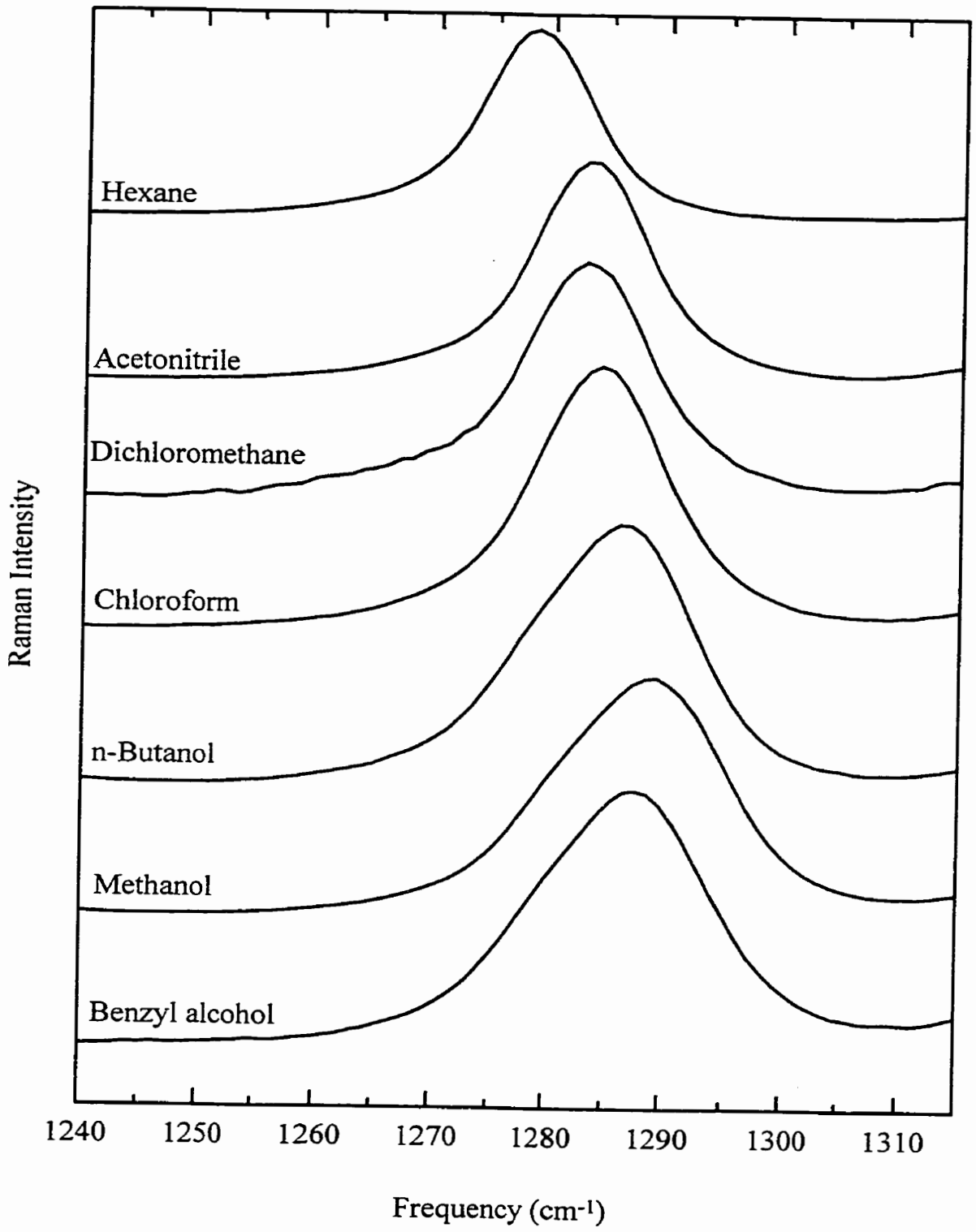
Hexane
Acetonitrile
Dichloromethane
Chloroform
n-Butanol
Methanol
Benzyl alcohol
Raman Intensity
1240
1250
1260
1270
1280
1290
1300
1310
Frequency (cm-1)

Figure 3.5- As in Figure 3.2, but for the OCO bend of DMABEE.

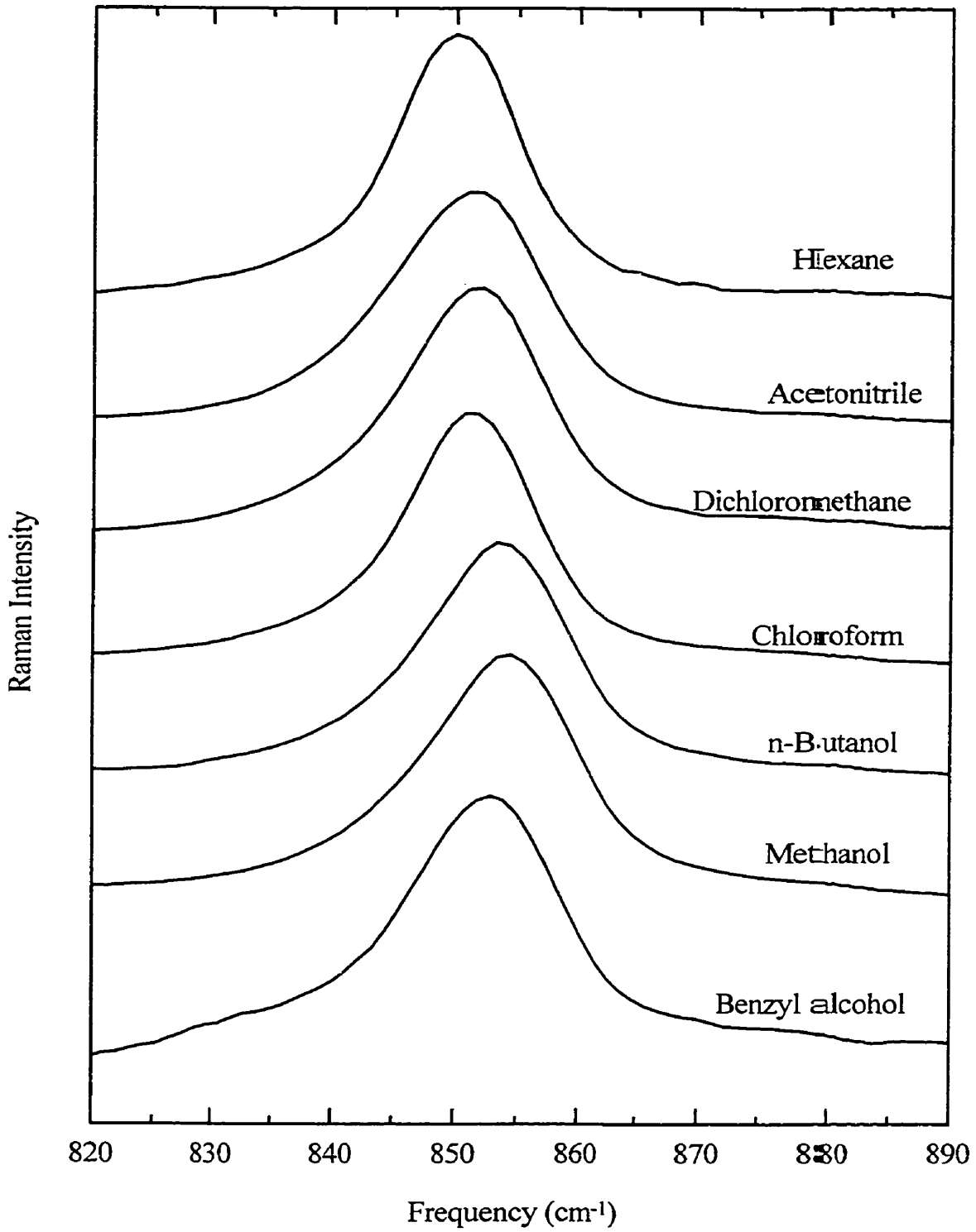
Hexane
Acetonitrile
Dichloromethane
Chloroform
n-Butanol
Methanol
Benzyl alcohol
Raman Intensity
820
830
840
850
860
870
880
890
Frequency (cm-1)

Table 3.2 Frequency shift of DMABEE vibrations.

Solvent	APAN	C=O stretch $\Delta(\Delta\upsilon)$ (cm^{-1})	C-O stretch $\Delta(\Delta\upsilon)$ (cm^{-1})	OCO bend $\Delta(\Delta\upsilon)$ (cm^{-1})
Hexane	-3.3	16.3	-4.7	-2.3
Diethyl ether	2.5	11.7	-3.6	-2.0
Benzene	11.4	4.7	-3.3	-1.7
1,4-Dioxane	11.9	4.3	-2.7	-1.7
Dimethylformamide	15.1	1.7	-1.0	-1.0
Acetonitrile	17.3	0.0	0.0	0.0
Dichloromethane	23.2	-4.7	0.0	0.0
Chloroform	24.9	-6.0	1.7	1.0
t-Butanol	31.2	-11.0	3.3	2.0
2-Propanol	33.7	-13.0	4.0	2.7
Hexanol	36.2	-15.0	3.0	2.0
Pentanol	36.2	-15.0	3.7	2.0
n-Butanol	36.2	-15.0	3.7	2.3
Propanol	36.6	-15.3	4.3	2.3
Ethanol	37.5	-16.0	4.0	2.0
Methanol	38.8	-17.0	6.0	2.7
d4-Methanol	40.0	-18.0	6.0	2.7
Benzyl alcohol	45.4	-22.3	4.7	2.3

In this table, APAN is the apparent acceptor number. The reported frequency shifts in cm^{-1} were determined as $\Delta(\Delta\upsilon) = \Delta\upsilon$(solvent) - $\Delta\upsilon$(acetonitrile), and are accurate to ± 0.5 cm^{-1}.

(hydrogen bond electron donor) effectively results in electron density shifting from the C=O bond to the solvent as the acceptor number increases, resulting in a decreased C=O bond order. However, the C-O stretching and OCO bending force constants increase slightly as a result of this electron density shift, due to increased delocalization of the lone pairs on the C-O oxygen and the increased equivalence of the bond orders. It is these bond order changes that cause the observed frequency shifts.

However, an additional complication is evident in the C=O stretching band as the solvent acceptor number increases; the band splits into two peaks. This splitting is attributed to a solvent-sensitive Fermi resonance between the C=O stretch and the first overtone of the OCO bend. As the solvent molecule hydrogen bonds to the solute, the C=O stretch fundamental frequency decreases and the first overtone OCO bend frequency increases, causing these two modes to go into Fermi resonance. However, as the solvent acceptor number continues to increase, the Fermi resonance is eventually lost and the two peaks re-coalesce into one. Fermi resonance between the C=O stretch fundamental and the first overtone of the putative Ph-C stretch around 880 cm^{-1} has been cited as the cause of the observed splitting in IR spectra of *para*-substituted benzoyl chlorides with the magnitude of splitting increasing with the substituent's increasing ability to donate electrons (21).

The unusually high frequency shift of the C=O stretch of DMABEE in benzyl alcohol is possibly due to a synergistic interaction between π–π stacking and hydrogen bonding (Figure 3.7). This could result from a solute-solvent ground state complex formation, in which a benzyl alcohol molecule lies above and parallel to DMABEE. The resulting π-π interaction amplifies the C=O stretch frequency shift compared to the effect of hydrogen bonding alone. A similar complex with benzene would have less effect on the shift due to

Figure 3.6 - Schematic of the proposed interactions between DMABEE and solvent. "SH" represents solvent with a potential hydrogen-bonding hydrogen.

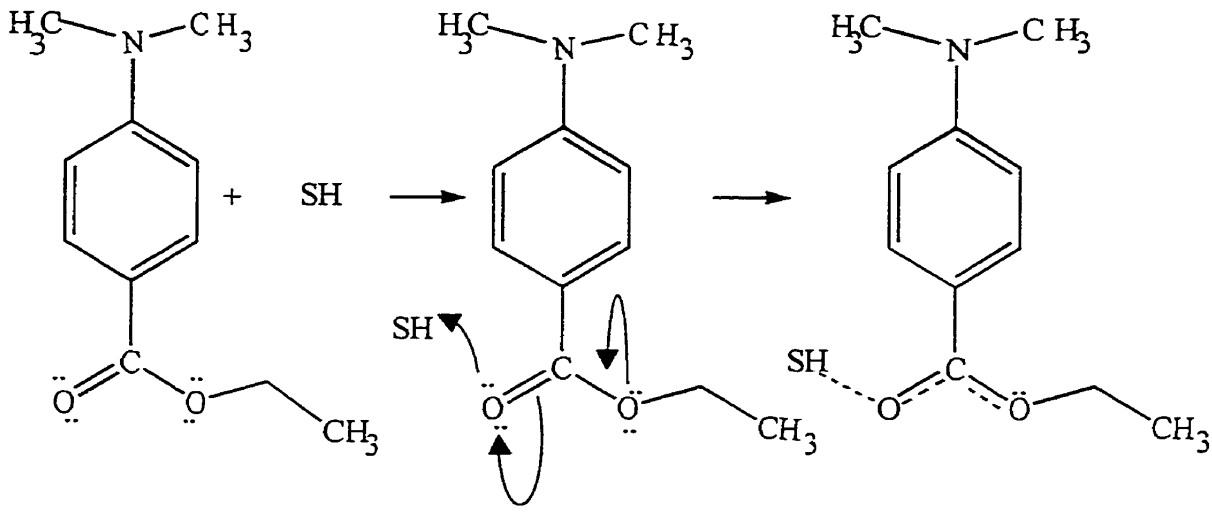
H3C
N
CH3
+
SH
SH
SH
O
O
O
CH3

Figure 3.7 - An illustration of the π-π interactions causing the anomalous behavior of benzyl alcohol.

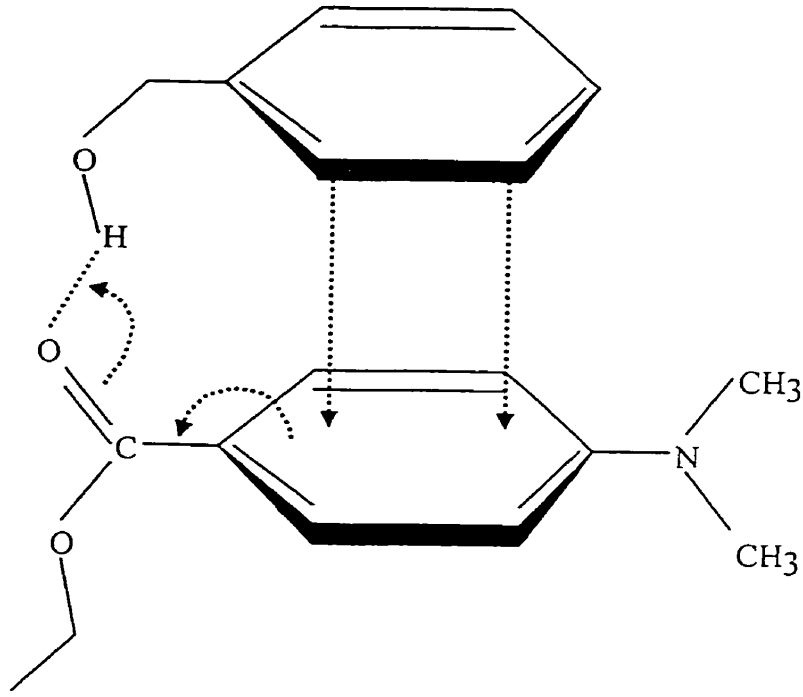
O
H
O
C
O
N
CH3
CH3

its lower ability to hydrogen bond. Similar solute-solvent complexes in the excited state have been reported for covalently-linked donor-acceptor molecules (8,9). Thus, Raman spectroscopy provides a sensitive means for discriminating the effects of solute-solvent complex and TICT state formation on the observed dual fluorescence of these molecules.

3.4 Conclusion

The Raman spectra presented in this chapter show that the interaction between DMABEE and solvent occurs primarily at the ester end of the molecule, specifically with the C=O moiety. The C=O stretch splits into a doublet due to Fermi resonance involving the first overtone of the OCO bend. The strength of the solvent-DMABEE hydrogen bond is the primary interaction responsible for modulating the energies of these interacting vibrational states. However, the anomalous shift of the C=O stretch in benzyl alcohol indicates that the vibrational frequencies are also differentially sensitive to π-π interactions. Thus, Raman spectroscopy allows the determination of the effect of different intermolecular interactions on ground state structure

3.5 References

1. Z. Grabowski, K. Rotkiewicz, A. Siemiarczuk, D. Cowley and W. Baumann, *Nouv. J. Chim.* **3,** 443 (1979).

2. K. Rotkiewicz and W. Rubaszewska, *Chem. Phys. Lett.* **70,** 444 (1980).

3. J. Lipinski, H. Chojnacki, Z. Grabowski and K. Rotkiewicz, *Chem. Phys. Lett.* **70,** 449 (1980).

4. W. Rettig, *Angew. Chem. Int. Ed. Engl.* **25,** 971 (1986).

5. Y. Wang and K. Eisenthal, *J. Chem. Phys.* **77,** 6076 (1982).

6. J. Hicks, M. Vandersall, Z. Babarogic and K. Eisenthal, *Chem. Phys. Lett.* **116,** 18 (1985).

7. J. Hicks, M. Vandersall, E. Sitzmann and K. Eisenthal, *Chem. Phys. Lett.* **135,** 413 (1987).

8. E. Chandross, in: The Exciplex, eds. M. Gordon and W. R. Ware (Academic Press, New York, 1975) p.175.

9. R. Visser, P. Weisenborn, C. Varma, M. de Haas and J. Warman, *Chem. Phys. Lett.* **104,** 38 (1984).

10. T. Soujanya, G. Saroja and A. Samanta, *Chem. Phys. Lett.* **236,** 503 (1995).

11. A. Myers and A. Johnson, *J. Phys. Chem.* **100,** 7779 (1996).

12. Y. Jung, J. Kang, S. Seo and M. Lee, *Bull. Korean Chem. Soc.* **17,** 128 (1996).

13. B. Britt, J. McHale and D. Friedrich, *J. Phys. Chem.* **99,** 6347 (1995).

14. E. Fraga, M. Webb and G. Loppnow, *J. Phys. Chem.* **100,** 3278 (1996).

15. E. Hester and M. Forster, *J. Chem. Soc., Faraday Trans. 2* **77,** 1535 (1981).

16. V. Gutmann, The Donor-AcceptorAapproach to Molecular Interactions (Plenum,

New York, 1978).

17. F. Riddle and M. Fowkes, *J. Am. Chem. Soc.* **112,** 3259 (1990).

18. R. Weast, Handbook of Chemistry and Physics (CRC Press, 53rd Ed. 1972-1973).

19. K. Dimroth, T. Siepmann, F. Bohlmann and C. Reinchardt, *Liebigs Ann. Chem.* **661,** 1 (1963).

20. J. Kamlet, M. Abboud and R. Taft, *J. Am. Chem. Soc.* **99,** 6027 (1977).

21. C. Rao and R. Venkataghavan, *Spectrochim. Acta* **18,** 273 (1962).

Chapter 4- Conclusions and Future Work

4.1 The Novel Divided Cell

A precise, accurate, and simple method for quantitating Raman and resonance Raman intensities with an external standard using a novel four nuclear magnetic (NMR)-tube holder has been developed. This cell has advantages over previous designs of divided cells (1-4). Raman and resonance Raman scattering experiments done using the holder and using a single tube holder compared well. The relative Raman intensities in a 1:1 mixture of benzene and chloroform taken in the single holder were within 6% of those of the pure solvents taken with the four NMR-tube holder. The resonance Raman scattering cross-section of chromate was determined to be within 6% of the value obtained from a single-tube holder. This difference is within the random error of measurements associated (2,5-9) with quantitation of Raman and resonance Raman cross-sections. All of these errors in accuracy and precision between the four nuclear magnetic resonance tube holder and a single tube holder are within the errors normally associated with the quantitative measurement of Raman cross-sections. The results demonstrated that the 4-tube spinner yielded precise and accurate results for Raman and resonance Raman spectra.

Despite the good precision and accuracy, two problems were encountered with the new design of the divided cell. These were, a low signal-to-noise ratio and artifacts from stray light. While the spectral quality obtained with transparent solutions was quite good, the signal-to-noise ratio becomes important when dealing with absorbing and fluorescing molecules as was used in the work described in this thesis. The signal-to-noise ratio is lower with the 4-tube holder because the analyte population in the probed volume in the sample varies more with time compared to the single tube spinner. Due to different axes

of rotation, for the 4-tube spinner, the sample is exposed to the laser beam less than half of the total time of spectral acquisition compared to the single tube spinner for which the sample is exposed all the time. This can be improved by longer exposure periods of the 4-tube holder compared to the single holder. To further increase the sample volume and also the exposure time of the sample, the design of the cell could be improved by increasing the number of tubes from the current four to a higher value. The other problem encountered with the 4-tube spinner results from the material used in making the holder. When used to obtain data in the deep ultraviolet region, the exciting laser beam increased the amount of Rayleigh scattering from the samples, primarily due to scattering from the holder. Since most materials will absorb in the UV region and cause scattering, this may be hard to fix. However, such artifacts are easily removed by taking a blank of the holder and subtracting this from the sample spectrum or by minimizing the amount of the holder seen by the exciting laser. All of the above problems in cell design can be eliminated by making the holder out of quartz glass or some other material which doesn't contribute significant Raman scattering or stray light artifacts. However this would be a formidable technical task.

4.2 Interactions of Ethyl 4-(dimethylamino)benzoate with Solvents

The Raman spectra reported in this thesis show that the interaction between DMABEE and solvent occurs at three vibrations whose frequencies shift with increasing solvent acceptor number. These were the C=O stretch around 1690 cm^{-1}, C-O stretch around 1280 cm^{-1}, and OCO bend around 850 cm^{-1} (10). A model has been proposed to describe

the molecular nature of the observed behavior based on solute-solvent hydrogen bonding and π-π interactions. Hydrogen bonding between the solvent and DMABEE appears to be the main interaction. Interaction between the solvent (electron acceptor) and DMABEE molecule (electron donor) results in bond order changes at the ester end of DMABEE. As the solvent acceptor number increases, the C=O bond order decreases whereas those of the C-O stretching and OCO bending modes increase slightly. These bond order changes cause frequency shifts to low and high frequencies, respectively, as the solvent acceptor number increases. In addition, a large shift in the frequency of the C=O stretch in benzyl alcohol occurs due to the vibrational frequencies being differentially sensitive to π-π interactions.

Future work to confirm the interactions at the ester end of the DMABEE molecule could be done with model compounds in which the ester group is replaced. This can be done with compounds such as 4-(dimethylamino)benzene methyl ketone and N,N-dimethylaniline. Similar interactions as those for DMABEE would be expected for the ketone while no such interactions would be expected to occur with the N,N-dimethylaniline. Though benzene as a solvent was used in this work, its effect on π-π stacking interactions was not as pronounced as in benzyl alcohol. To further establish the level of the π-π stacking interactions, more work would be required for aromatic solvents that can also hydrogen bond strongly. This can be done with solvents such as aniline, 2-anilinoethanol, phenol, substituted benzyl alcohols such as *ortho* or *meta* methoxybenzyl alcohols, etc. The number of aromatic rings in the solvent can also be increased and the results compared with those of the single benzene ring already undertaken in this work.

These results suggest that Raman spectroscopy as a vibrational technique provides a mode-specific measure of solute-solvent interactions. They also show that one can obtain Raman spectra of ethyl 4-(dimethylamino)benzoate (DMABEE) and that the ground state dynamics are affected by the solvent. However, the main goal of this work was to determine which of the TICT models was more appropriate. To probe the excited-state dynamic, resonance Raman spectroscopy would be an ideal technique to use.

Preliminary UV resonance Raman experiments yielded reasonable quality spectra with excitation wavelengths throughout the putative charge transfer absorption band. The spectral quality was sufficient for the quantitative determination of Raman cross-sections and extraction of the excited-state structure and dynamics. UV resonance Raman spectra of DMABEE in methanol at 3 excitation wavelengths are shown in Figure 4.1. These results are encouraging for a definitive elucidation of the excited-state processes which give rise to the observed dual fluorescence. Preliminary resonance Raman spectra of DMABEE in tetrahydrofuran at ten wavelengths within the absorption band also indicated that the observed vibrational modes are enhanced by electronic transition(s) centered at 240 and/or 300 nm, suggesting that dynamics in multiple electronic states may be important.

More resonance Raman work is required to determine unequivocally which modes are being enhanced by which electronic transition(s). In order to determine the excited-state dynamics, further resonance Raman work will be required to measure the resonance Raman excitation profiles and extract the excited-state structure and dynamics. Once these issues are settled, more work would be required to determine the role of the

Figure 4.1 - Resonance Raman spectra of DMABEE obtained at 3 excitation wavelengths. (A) 275 nm, (B) 300 nm, and (C) 351 nm.

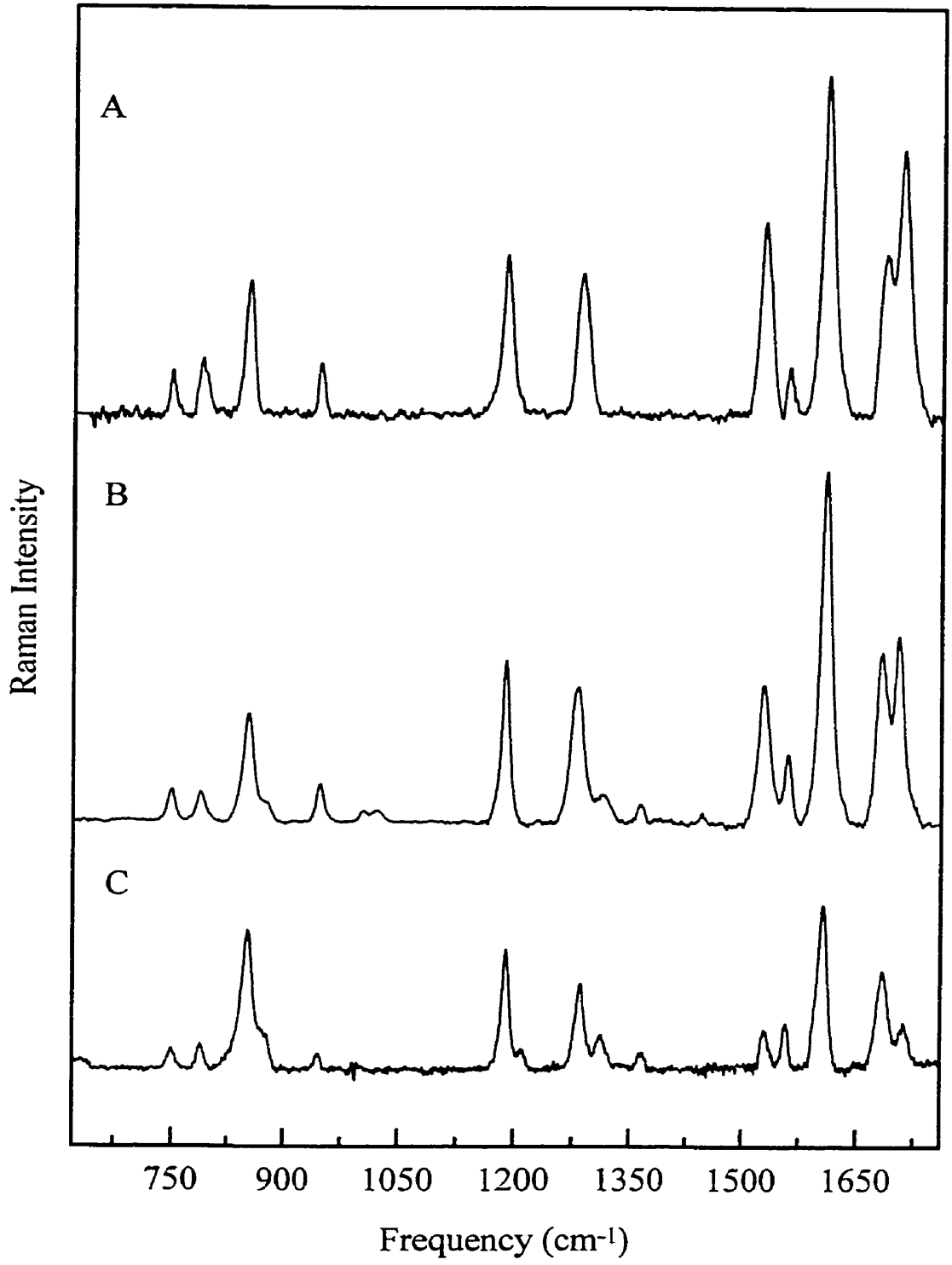
A
B
C
Raman Intensity
750
900
1050
1200
1350
1500
1650
Frequency (cm-1)

environment in the excited state by comparing the excited state effects in the various solvents.

4.3 References

2. H. Eysel and J. Bertie, *J. Raman Spectrosc.* **19**, 59 (1988).

1. I. Tsukamoto, H. Nagai and K. Machida, *J. Raman Spectrosc.* **17**, 313 (1986).

3. B. Bussian and C. Sander, *Biochem.* **28**, 4271 (1989).

4. W. Kiefer, *Appl. Spectrosc.* **27**, 253 (1973).

5. E. Fraga, M. Webb and G. Loppnow, *J. Phys. Chem.* **100**, 3278 (1996).

6. F. Markel, N. Ferris, I. Gould and A. Myers, *J. Am. Chem. Soc.* **114**, 6208 (1992).

7. G. Loppnow and R. Mathies, *Biophys. J.* **54**, 35 (1988).

8. K. Schomacker, J. Delney and P. Champion, *J. Chem. Phys.* **85**, 4240 (1986).

9. M. Trulson and R. Mathies, *J. Chem. Phys.* **84**, 2068 (1986).

10. E. Hester and M. Forster, *J. Chem. Soc., Faraday Trans. 2* **77**, 1535 (1981).